# Feasibility of Using Power Steering Pumps in Small-Scale Solar Thermal Electric Power Systems

By
Cynthia Lin

SUBMITTED TO THE DEPARTMENT OF MECHANICAL ENGINEERING IN PARTIAL FULFILLMENT OF THE REQUIREMENTS FOR THE DEGREE OF

BACHELOR OF SCIENCE IN MECHANICAL ENGINEERING
AT THE
MASSACHUSETTS INSTITUTE OF TECHNOLOGY

[February 2008]
JANUARY 2008



Signature of Author: _____
Department of Mechanical Engineering
31 January 2008

Certified by: _____
Ahmed F. Ghoniem
Professor of Mechanical Engineering
Thesis Supervisor

Accepted by: _____
John H. Lienhard V
Professor of Mechanical Engineering
Chairman, Undergraduate Thesis Committee

THIS PAGE IS INTENTIONALLY LEFT BLANK

# Feasibility of Using Power Steering Pumps in Small-Scale Solar Thermal Electric Power Systems

by
Cynthia Lin

Submitted to the Department of Mechanical Engineering on January 31, 2008
in partial fulfillment of the requirements for the
Degree of Bachelor of Science in Mechanical Engineering

## Abstract

The goal of this study was to determine performance curves for a variety of positive displacement pumps in order to select an efficient and low cost option for use as a boiler feed pump in a 1-$kW_e$ organic Rankine cycle (ORC) system built by the Solar Turbine Group in Lesotho. The pumps tested included OEM plunger and piston pumps, and rotary vane-type power steering pumps purchased from a junk yard. Motor speed and torque were measured at different flow rates to determine the power consumed to move fluid in the prescribed pressure regime. The test station was designed to pump deionized water; it was intended that measurements and calculations would then be non-dimensionalized and used to predict the ORC working fluid's properties. Unfortunately, deionized water caused the power steering pump shafts to seize; the efficiencies were below anticipated and the pumps were unable to operate under the specified pressures. It was discovered, after WD-40 was added to the water, that power steering pumps performed best when moving fluids with more lubricity. The optimal pump was selected based on how the pump efficiency affected the overall ORC system efficiency, defined as the electrical work output divided by the heat input, and the net electric power output. Power steering pumps achieved efficiencies between 34%-54% under the desired ORC operating conditions with water-oil emulsion as the working fluid. For that pump efficiency range, the overall solar thermal electric ORC system efficiency would be 7.4%-8.5% and the overall system cost would be USD 4.59-5.27 per installed Watt. Made specifically for pumping hydroflurorcarbons, the working fluid used in STG's ORC, the OEM Dynex pump exhibited poorer performance than predicted. The pump efficiency of 31% gave a system efficiency of 7.1% and a cost of USD 6.40 per installed Watt. The OEM water piston and plunger pumps made by Hypro achieved efficiencies of 70% and 81%, respectively, under the same ORC operating conditions described above. For those pump efficiencies, the overall system efficiencies would be 9.0% and 9.2% and the costs would be USD 4.58 and 4.63 per installed Watt, respectively. The most optimal pump is the HyproPiston pump; although it costs nearly six times that of a power steering pump, the overall system cost is lower when normalized over the power output.

Thesis Supervisor: Ahmed F. Ghoniem
Title: Professor of Mechanical Engineering

THIS PAGE IS INTENTIONALLY LEFT BLANK

# Acknowledgements

I am extremely grateful to have had the opportunity to be a part of the MIT community. My experiences at the Institute have been challenging, yet fun, memorable, and wonderfully rewarding. I would like to express my sincere appreciation to the following people who made my involvement in this project possible:

- My thesis supervisor, Professor Ahmed Ghoniem, for providing invaluable feedback and guidance throughout the project.
- The Solar Turbine Group, in particular, Matthew Orosz and Amy Mueller. Their passion for helping rural communities in developing countries is inspiring. Matt's guidance has proven to be an indispensable, particularly in designing, machining, and troubleshooting. Amy has been an invaluable technical resource, particularly with anything involving electrical engineering.
- The Ralph M. Parsons Laboratory
- Central Machine Shop
- And finally, my family and friends for their years of love, encouragement and support.

# Table of Contents

# List of Tables

# List of Figures

# Chapter 1 Introduction and Background

Rural communities in developing countries often do not have access to electricity grids. A number of decentralized power generation schemes, such as diesel engines, have been examined and deployed around the world. However, there are few cost-effective, clean power generation schemes that have been implemented. The goal of this study is to determine performance curves for a variety of pumps in order to optimize a low cost solar thermal, organic Rankine cycle system built by the Solar Turbine Group in Lesotho.

## *1.1 Motivation*

The Solar Turbine Group (STG) is a non-profit organization founded by MIT students whose vision is to provide rural areas of the developing world with access to energy (electricity, heating, cooling) via solar technologies. To date, it has installed two field prototype solar-trough concentrators in Lesotho capable of producing hot water and driving a heat engine. The engine is a solar thermal-fueled organic Rankine cycle (ORC) using HFC-245fa as a working fluid. Initial field testing of the ORC showed that it was net energy negative; more power was required to run the system than it produced. After observing a high current draw from the feed pump motor during operation, the initial diagnosis was low efficiency of the fluid machinery. Whereas a notable feature of a properly functioning Rankine cycle is the relatively low energy cost of condensate pumping compared to expander output, the energy draw for condensate pumping in the Lesotho ORC systems was greater than expander output and represented a low efficiency (below 10%) for the pump. The current phase of research is to test and identify commonly available components (low-flow high-pressure pumps) to replace the current system feed pump, and to characterize the efficiency of expanders. Replacing the system's existing components with optimal mechanical component (pumps and expanders) will allow the system to be more efficient in providing hot water and electricity with less wasted energy.

The objectives of this project are:

- To build a pump testing station
- To test a variety of automotive power steering pumps and specialized OEM pumps and produce pump performance curves under operating conditions of the ORC
- To identify optimal boiler feed pump to increase system efficiencies at the lowest cost option

## *1.2 Description of Solar Thermal Power Plants*

Renewable energy technologies are often regarded as expensive investments. However, rising $CO_2$ emissions from fossil fuel use and global warming concerns have inspired consumers, companies and research institutes to take a closer look at harnessing solar energy.

Solar power generation is appealing because its uses a renewable and non-exhaustible energy source. The sun has been and will continue producing energy for billions of years. Solar energy can be converted into useful forms of energy, such as electricity and heat, and has been harnessed since at least the seventh century BC. In the eighteenth century, a Swiss scientist built the first solar collector, the "hot box," to test a common observation that glass could trap solar heat. Since then, a vast range of solar-electric and solar-thermal applications have been developed. The amount of solar radiation that reaches the earth's surface varies depending on location, time of day, season of the year, and weather conditions. Because sunlight is disperse and delivers very little energy (~ 4 $kW/m^2$-day) to a given space at a given time, large collector areas are necessary to compensate for the low density of solar radiation.

There are two widely practiced methods of converting solar energy into electricity: photovoltaic (PV) cells and solar thermal power plants. Photovoltaic cells are semiconductor devices that convert sunlight directly into electricity. Typical solar thermal power plants absorb sunlight as thermal energy, which heats a working fluid to produce steam. The steam is then fed into a steam turbine electric generator, similar to those used in typical fossil fuel power plants. The three most common types of solar thermal collector systems are: troughs, solar dishes, and solar power towers (EIA, 2007).

Despite over 25 years of experience with solar thermal power, the technology has had limited success in the energy market. This can in part be attributed to the low cost of power generation using fossil fuels, and to the relative immaturity of solar thermal technologies compared to traditional power blocks that have been incrementally improved and optimized over the past 120 years. The ability to characterize the performance of solar thermal power systems is a prerequisite for the development of economically viable designs. The properties of organic Rankine cycles have been cited as suitable options for solar power generation using low temperature thermal energy sources (NREL, 2007). Thermal energy storage allows the power plant output to be tailored to user demands, but is often an expensive option (McMahan, 2006).

Small hybrid solar power systems (HSPS), using parabolic solar concentrators in combination with fossil fuels for cogeneration purposes, are increasingly the focus of development. They are generally less than a few tens of $kW_e$. Kane et al (2003) describes design parameters of a small HSPS (Kane et al, 2003). The plant contains two rows of solar collectors, two superposed ORC equipped with a scroll hermetic expander-generator, and a diesel engine. In hybrid mode, additional heat is supplied by heat recovery from the exhaust gases of the diesel engine in series with the solar network and by a separate network recovering heat from the cooling of the engine block at an intermediate temperature level, as shown in Figure 1-1 (Kane et al, 2003).

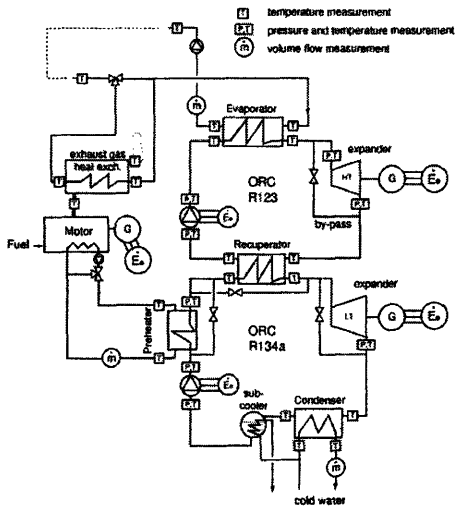


**Figure 1-1: Simplified Flowsheet of the SPS power unit**

The electric power output as a function of the heat supplied to the evaporator, for a heat supply temperature range of 130 to 165 °C, as shown in Figure 1-2. The overall superposed cycle efficiency is cited as 14.1% for power outputs up to 10 $kW_e$ from temperature supply up to 165°C (Kane et al, 2003).

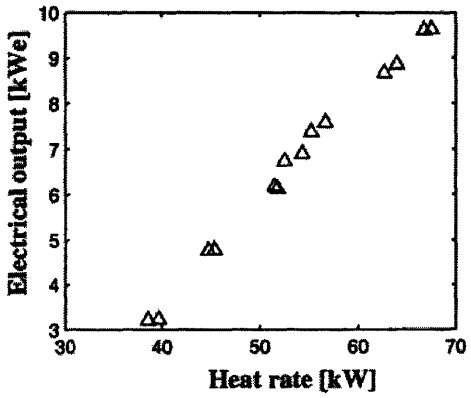


**Figure 1-2: Electric power output as a function of the heat supplied to the evaporator**

## *1.3 Organic Rankine Cycle*

An organic Rankine cycle is a closed-circuit thermodynamic cycle commonly used by power stations to generate electricity. Conventional Rankine cycles use steam as the working fluid while organic Rankine cycles use hydrocarbon-based compounds. Examples of these hydrocarbons include Freon, butane, ammonia, and other refrigerants. These substances boil at temperatures below the boiling point of water, which is advantageous in a solar-based system. After the refrigerant reaches its boiling point, it is in a high-pressure vapor state and can be used to drive an expander to do work.

A Rankine cycle is a specific example of the Carnot cycle. In a Rankine cycle, working fluid is heated in a heat exchanger, or boiler, to form pressurized gas. The gas is then expanded through a series of turbines, which spin. The turbines drive a generator and convert the mechanical work into electricity. After the gas exits the turbines, it enters another heat exchanger, known as a condenser. The gas is cooled as it gives off its heat to another fluid stream. After being condensed, the working fluid is pumped back into the boiler. The organic Rankine cycle, like the standard Rankine cycle, consists of a boiler, a turbine, a condenser, and a pump, as shown in Figure 1-3 below (Soffientini, 2003).

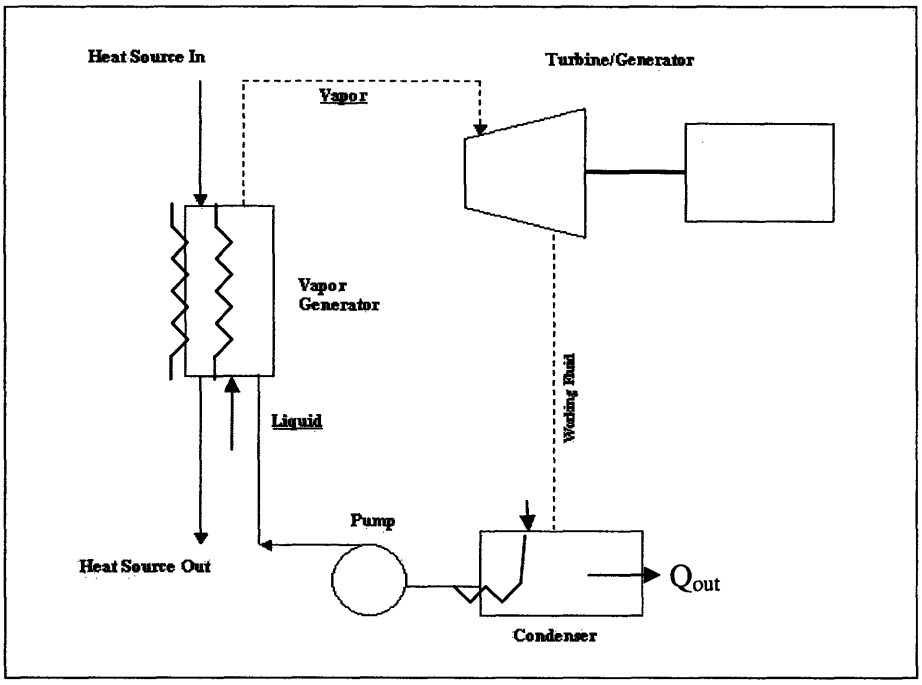


**Figure 1-3:** Simple Organic Rankine Cycle System Diagram

A basic ideal Rankine cycle is a four-stage process (Wu, 2004):

- Isobaric heat addition (across boiler)
- Isentropic expansion (across turbine)
- Isobaric heat removal (across condenser)
- Isentropic compression (across pump)

A typical temperature-entropy (T-S) diagram for a Rankine cycle is shown below in Figure 1-4 (Tester et al, 2005). The Rankine power cycle is marked by (ABCDEFA) and the Carnot idealization is marked by (AB'EFA). The dashed curve defines coexistence of working fluid vapor and liquid.

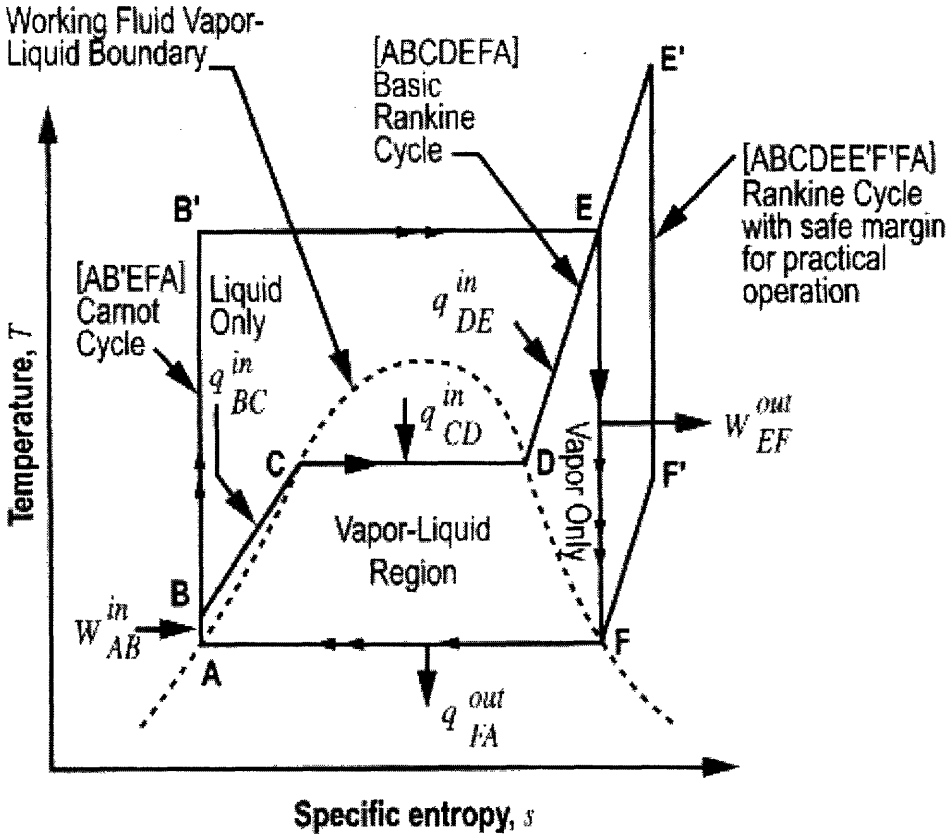


**Figure 1-4: T-S Diagram for a typical Rankine cycle**

The working fluid being used in STG's solar micro-generator systems is HFC-245fa, 1,1,1,3,3-pentafluoropropane. ORC systems favor the HFC-245fa because it exhibits physical and thermodynamic properties favorable for refrigeration applications. The manufacturer Honeywell describes HFC-245fa as having a number of applications, such as foam blowing agent, solvent, aerosol, and organic Rankine cycles (Soffientini, 2003). The thermodynamic and physical properties are listed in Table 1-1.

**Table 1-1: Physical and thermodynamic properties of HFC-245fa**

| Properties of HFC-245fa | |
|---|---|
| **Chemical Name** | **1,1,1,3,3-pentafluoropropane** |
| **Molecular Formula** | **CF3CH2CHF2** |
| **Molecular Weight** | **134** |
| **Flammability Limits in Air @ 1atm** (vol.%)** | **None** |
| **Flash Point *** | **None** |
| **Water Solubility in HFC-245fa** | **1600 ppm** |
| **ASHRAE Safety Group Classification** | **B1** |

**Flashpoint by ASTM D 3828-87; ASTM D1310-86*
***Flame Limits measured at ambient temperature and pressure using ASTM E681-85 with electrically heated match ignition, spark ignition and fused wire ignition; ambient air.*

| Standard International Units* | | English Units* | |
|---|---|---|---|
| Boiling Point °C @ 1.01 bar | 15.3 | Boiling Point (°F) @ 1atm | 59.5 |
| Freezing Point °C @ 1.01 bar | <-107 | Freezing Point (°F) | <-160 |
| Critical Temperature** (°C) | 154.05 | Critical Temperature** (°F) | 309.29 |
| Critical Pressure** (bar) | 36.4 | Critical Pressure** (psia) | 527.9 |
| Critical Density** (m3/kg) | 517 | Critical Density** (lb/ft3) | 32.28 |
| Vapor Density @ Boiling Point (lb/ft3) | 5.921 | Vapor Density @ Boiling Point (lb/ft3) | 0.3697 |
| Liquid Density (kg/m3) | 1339 | Liquid Density (lb/ft3) | 83.58 |
| Liquid Heat Capacity (kJ/kg K) | 1.36 | Liquid Heat Capacity (Btu/lb °F) | 0.33 |
| Vapor Heat Capacity @ constant pressure, 1.01 bar (kJ/kg K) | 0.8931 | Vapor Heat Capacity @ constant pressure, 1atm (Btu/lb °F) | 0.218 |
| Heat of Vaporization at Boiling Point (kJ/kg) | 196.7 | Heat of Vaporization at Boiling Point (Btu/lb) | 84.62 |
| Liquid Thermal Conductivity (W/m K) | 0.081 | Liquid Thermal Conductivity (Btu/hr ft °F) | 0.0468 |
| Vapor Thermal Conductivity (W/m K) | 0.0125 | Vapor Thermal Conductivity (Btu/hr ft °F) | 0.0072 |
| Liquid Viscosity (mPa s) | 402.7 | Liquid Viscosity (lb/ft hr) | 0.9744 |
| Vapor Viscosity (mPa s) | 10.3 | Vapor Viscosity (lb/ft hr) | 0.025 |
| **Properties at 77 °F / 25 °C unless noted otherwise* | | | |
| ***NIST Refprop v 7.0* | | | |

The Barber-Nichols Engineering Company used a centrifugal pump in their design of an organic Rankine cycle and noted a peak pump efficiency of 27% at a peak pressure of 5.9 MPa and full system flow rate of toluene at 544 kg/hr (Barber and Boda, 1982).

## *1.4 The Solar Turbine Group*

The Solar Turbine Group (STG) is a non-profit organization based in Cambridge, Massachusetts. Since 2004, STG has been developing a solar thermal power system based on the organic Rankine cycle that would ultimately supply hot water, electricity, and refrigeration to communities in the developing world. The system harnesses solar energy via parabolic troughs and is made from commonly available automotive parts and plumbing supplies. STG's vision is to provide rural areas with access to affordable, locally customized, and distributed renewable forms of energy generation that would "improve productivity and quality of life without significantly increasing their carbon footprints." Figure 1-5 is a diagram summarizing STG's solar microgenerator scheme (STG International, 2007).

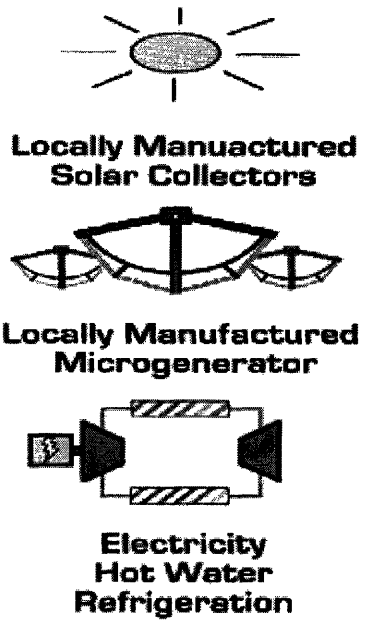


**Figure 1-5: Schematic summarizing STG's solar microgenerator scheme**

The primary goals of the Solar Turbine Group are (STG International, 2007):

- To provide energy access to rural villages, clinics, schools, and organizations of developing countries using their solar micro-generator
- To augment local knowledge and capacity through training in manufacturing and design
- To increase local economic activity through fostering local manufacture and dissemination
- To jump-start new ventures aimed at selling and maintaining STG-style micro-generator systems

### 1.4.1 The Technology

The current outputs of the system are electricity and hot water; the system may later be used for refrigeration via an absorption-chiller design. The system that STG has designed consists of three main components: the parabolic troughs, the organic Rankine cycle (ORC) engine, and the electrical control system. The parabolic troughs focus sunlight onto an evacuated Dewar tube at the trough's focal line. A thermal absorption fluid (glycol) circulates in the pipe, absorbs the sun's heat, and reaches 150° C at the end of the loop. The thermal absorption fluid then transfers heat to a working fluid (refrigerant) via a heat exchanger. The working fluid then drives an ORC engine to produce hot water and electricity, as described in previous sections. The system is designed to produce 600W to 1kW of electricity along with ~10kW of thermal outputs (e.g. hot water). In such a configuration, a 24 square-meter array of parabolic mirrors can produce up to 600L of hot water during a sunny summer day and approximately half as much on a sunny winter day

with fewer hours of sunlight. A schematic of the solar trough-ORC module is shown in Figure 1-6 (STG International, 2007).

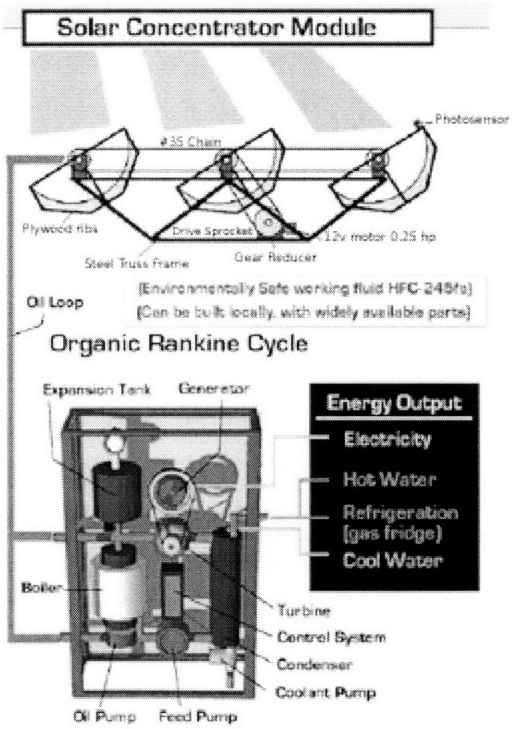


**Figure 1-6: Schematic of STG's Solar Concentrator-ORC Module**

### 1.4.2 Design Specifications

Below are STG's design specifications for its solar micro-generator (STG International, 2007):

Thermal Input
- Direct Sunlight
  - 800-1000 W/$m^2$, peak
  - 400-600 W/$m^2$, nominal
- 80-90% thermal collector efficiency

Thermal Output
- 800 W/$m^2$ peak thermal output
- 150° C max. temperature
- 24 $m^2$ array = 10 kW thermal, nominal

Electrical Output
- 1 kW electrical / 6 kW thermal (co-generation mode)
  - up to 15% thermal-electric efficiency
  - 2-10% solar-electric efficiency
- 13.6V DC output (12V DC battery charging)
- AC inverter component possible

Refrigeration Output
- Absorption-chiller refrigeration
  - 6 kW chilling capacity
- Electrical refrigeration
  - 3 kW chilling capacity
  - 6 kW thermal at 50° C

Figure 1-7 is a schematic of STG's ORC unit, shown without the air condenser.

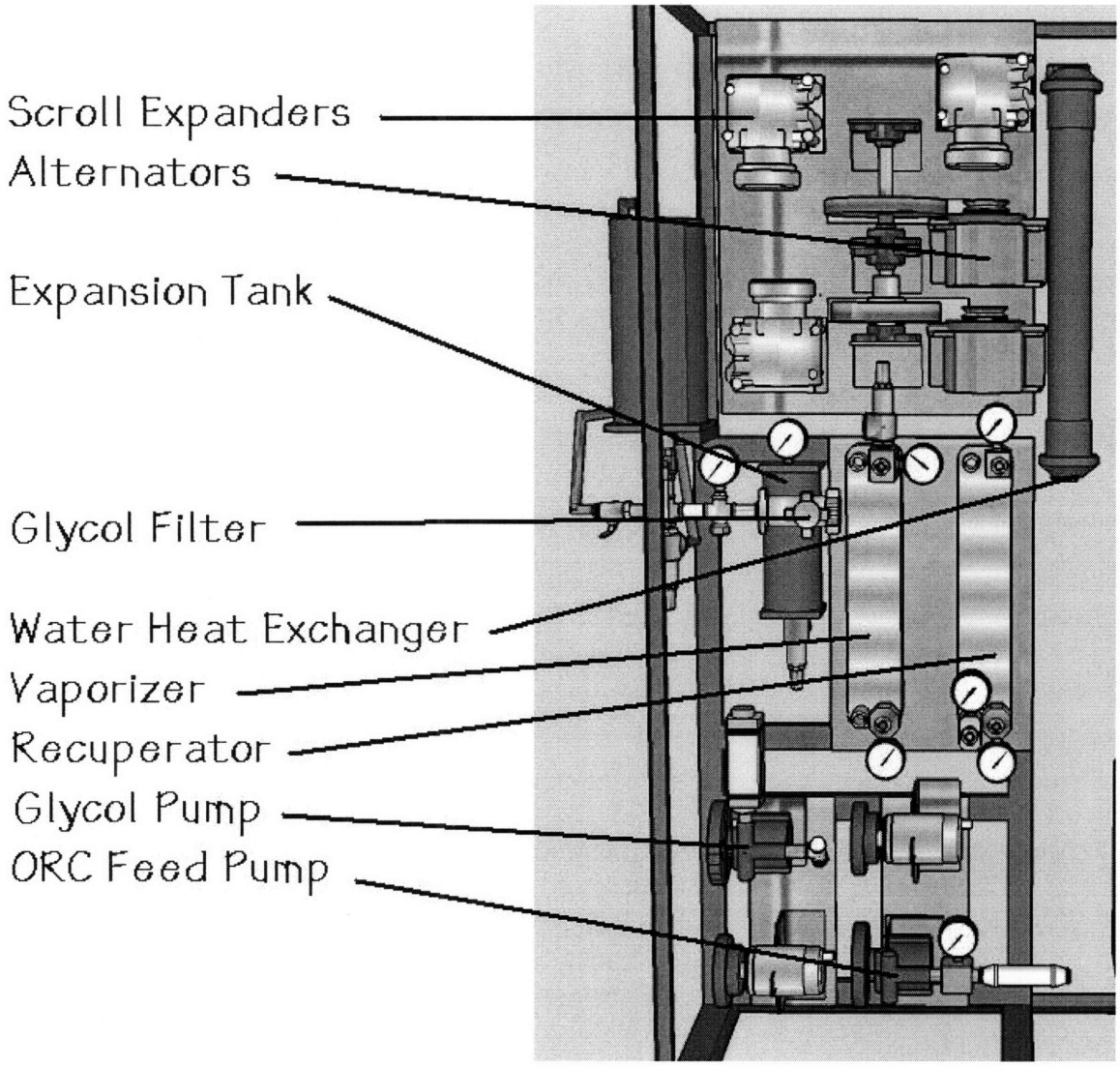


**Figure 1-7: Diagram of STG's ORC unit, without air condenser**

### 1.4.3 Project Implementations

Prototypes of the solar micro-generators are located at MIT (Cambridge, Massachusetts) and two locations in Lesotho, Bethel high school and the village of Ha Teboho. The Solar Turbine Group was awarded the World Bank Development Marketplace award in 2006, whereupon members of STG worked for 11 months to build and install the two pilot systems in Lesotho, located in southern Africa.

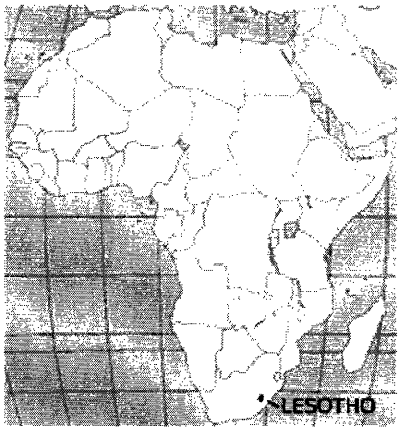


**Figure 1-8: Map of Lesotho (STG International, 2007)**

The first international field site is Bethel High School. The STG system installed at BHS is located near the girls' dormitory to provide hot water to their bathing facilities. Students from the villages and towns in the Phamong region of Lesotho attend this high school. Most students are housed in dormitories and have limited access to hot water, even during winters where temperatures drop significantly below freezing. Currently, a diesel generator that runs on fuel subsidized by the Lesotho Ministry of Education supplies electricity for four hours a day to a small computer lab.

The second international field site is the village of Ha Teboho, located near Bethel, just north of the Senqu River. The STG system installed at Ha Teboho is centrally located, approximately 10 meters from the community water tap, and currently provides on-demand hot water for the community to share. Upgrades to this system in Spring 2008 should add cell phone and battery charging capabilities.

A notable feature of a properly functioning Rankine cycle is the relatively low energy cost of condensate pumping, compared to the energy output by the expander. However, the energy draw for condensate pumping in the Lesotho ORC systems was greater than the energy output of the expander, representing a low efficiency (below 10%) for the pump. Since the expander power is less than the pump power, the pilot systems in Lesotho are energy negative, which means that more power is required to run the system than what is produced. The pumps and expanders used in the Lesotho systems are automotive components, which do not perform as efficiently as predicted under the ORC operating conditions. Thus, the motivations for this project are to characterize pump efficiencies.

## *1.5 Introduction to Pumps*

A pump is a machine used to move liquid through a piping system and to raise the pressure of the liquid (Volk, 2005). There are two broad categories of pumps: Positive Displacement Pumps and Centrifugal/Dynamic Pumps. This project focuses on pumps in the positive displacement family: reciprocating piston, reciprocating plunger, and rotary vane. Figure 1-9 is a diagram classifying the different types of pumps (Volk, 2005).

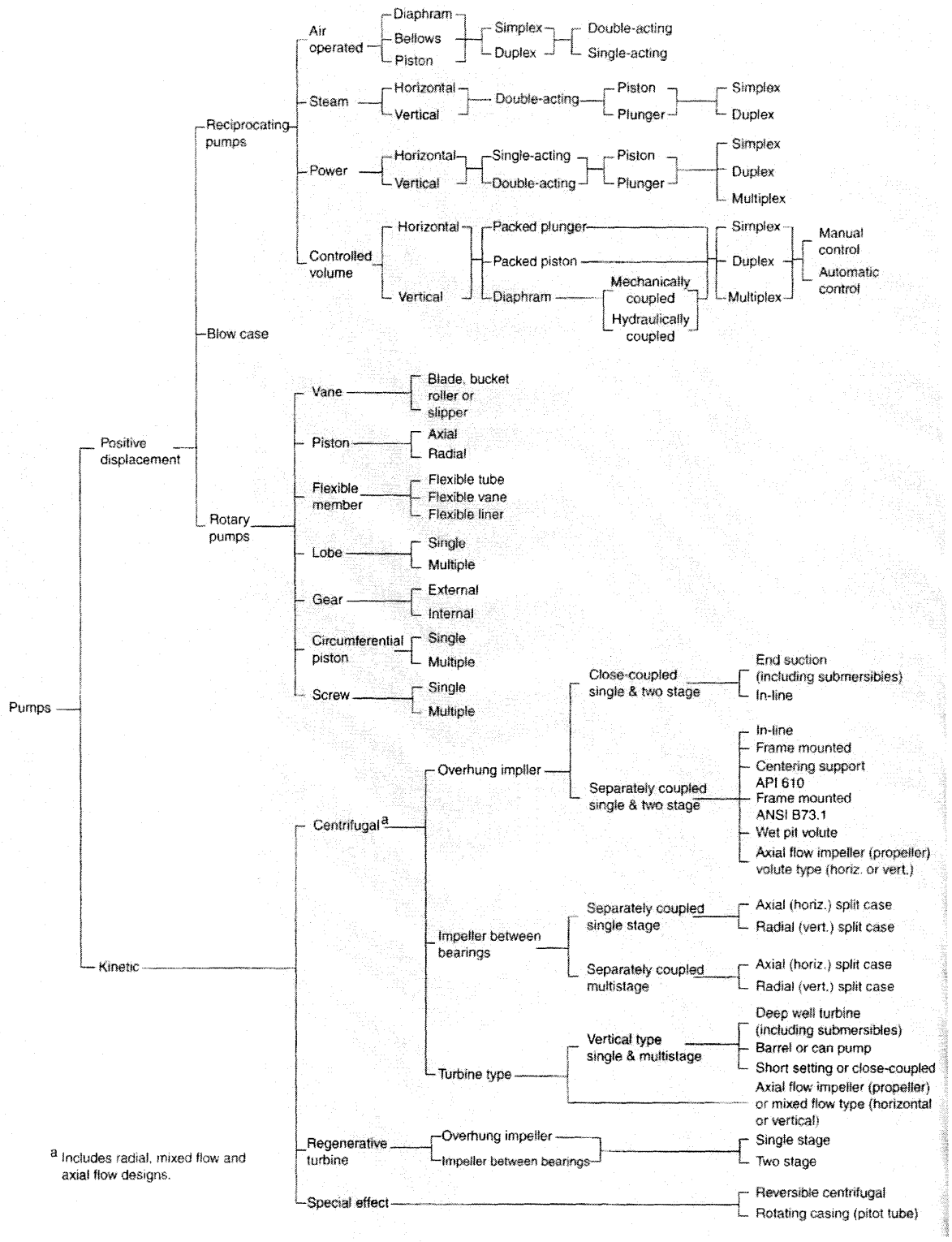


**Figure 1-9: Classification of Pumps**

The relative performance (pressure or head difference versus capacity or discharge) is different between positive displacement pumps and centrifugal pumps. Positive displacement pumps produce nearly constant flow rates and virtually unlimited pressure rise, with little effect of viscosity, at a constant shaft rotation speed. The flow rate of a positive displacement pump can only be varied by changing the displacement or the speed. In contrast, centrifugal pumps provide continuous constant-speed variation of performance. It provides near maximum pressure difference at zero flow (shutoff conditions) to zero pressure difference at maximum flow rate. Centrifugal pumps are adversely affected by high-viscosity fluids (White, 2003). These characteristics are shown in the expected performance curves in Figure 1-10 below (White, 2003).

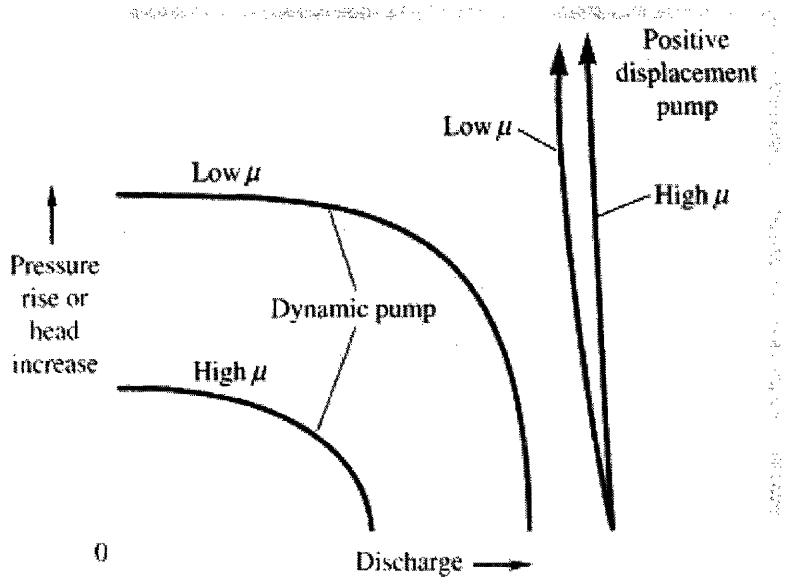


**Figure 1-10: Expected performance curve for dynamic and positive displacement pumps**

## 1.5.1 Centrifugal/Dynamic pumps

Centrifugal pumps, also known as dynamic pumps, are best suited for transfer applications that involve high flow rates, low pressure and low viscosity. They typically require priming. If they are filled with gas, they cannot suck up liquid below the inlet, thus requiring a gravity-feed setup. They can provide high flow rates of up to $1x10^6$ LPM, but only with moderate pressure rises of a few 100 kPa (White, 2003). Flow capacity is regulated by throttling and varying impeller speeds. The head created by a centrifugal pump depends upon the flow rate the fluid imparts on the impeller.

## 1.5.2 Positive Displacement Pumps

Positive displacement pumps use a mechanical force to push a fixed volume of fluid from the inlet through the outlet of the pump. The cavity on the suction side expands while the

cavity on the discharge side contracts. Energy is added to the pumped fluid periodically, whereas energy is added continuously to dynamic pumps. Positive displacement pumps are best suited for high-pressure, varying-pressure, or high-viscosity transfer applications. They are typically self-priming; they are able to create enough vacuum to draw fluid without assistance. Compared centrifugal pumps, positive displacement pumps are better able to produce the same flow at a given speed. They can operate at high pressures of up to $3x10^4$ kPa, but produce low flow rates of around 450 LPM (White, 2003). The capacity of a positive displacement pump is proportional to the pump speed. The maximum head is determined by the strength of the pump casing and the power available from the motor. There are two broad categories of positive displacement pumps: reciprocating pumps and rotary pumps.

## Reciprocating Pumps

The operational principle of a reciprocating pump is that a solid volume (piston, plunger, or diaphragm) will displace a liquid volume. Reciprocating pumps have a maximum operating pressure rating that largely depends on the application and the strength of the material. The basic conditions are the suction and discharge strokes. The head does not depend on the velocity the pump imparts on the fluid via the impeller. The capacity of the pump is proportional to the displacement of the pump over time. Factors affecting theoretical capacity of the pump: slip, volumetric efficiency. The mechanical efficiency of a piston or a plunger pump ranges between 80 and 95% depending upon speed, size, and construction.

**Piston pumps** use pistons to move media through a cylindrical chamber. The piston requires some form of actuation. It is usually driven thermally, pneumatically, hydraulically, or electrically. They are widely used in lower flow, moderate pressure (13.5MPa) applications.

**Plunger pumps**, also known as swash plate pumps, use plungers to move media through a cylindrical chamber. The actuation sources are the same as for piston pumps. They can typically withstand pressures up to 200 MPa. The sealing system (rings, packing, etc) for piston pumps are attached to the piston and thus move with it during its stroke. The sealing systems of plunger pumps are stationary and the plunger moves through it during its stroke.

Figure 1-11 is a schematic design of a reciprocating piston or plunger pump (White, 2003).

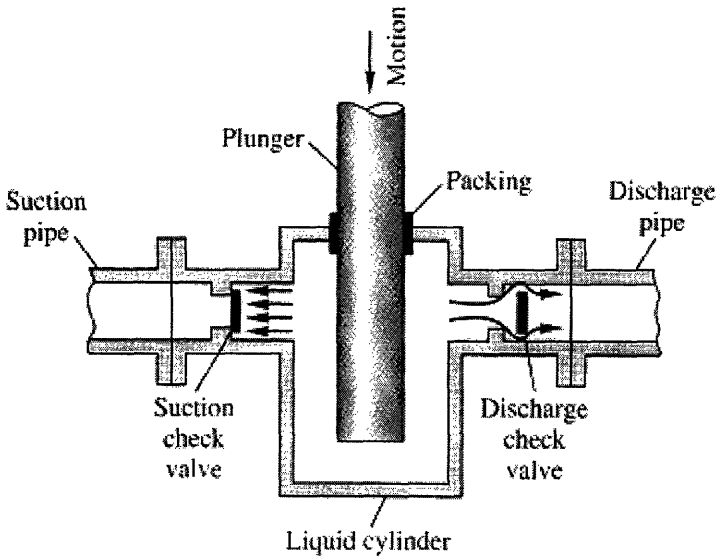


**Figure 1-11: Schematic diagram of a reciprocating piston or plunger pump**

**Diaphragm pumps** use flexible membranes to displace pumped fluid. It is self-priming. It does not require a sealing system and thus operates leak-free.

Affinity Laws for Positive Displacement Pumps (McNally Institute, 2008)
Flow - Flow varies directly with a change in speed. If the rotational speed is doubled, flow is also doubled.

Pressure - Pressure is independent of a change in speed. The pressure generated at any given rotational speed will equal the amount required to support flow, plus efficiency losses.

Horsepower - Horsepower varies directly with a change in speed. If the rotational speed is doubled, then twice as much power will be required.

NPSHr - Net Positive Suction Head required varies as the square of a change in speed. If the rotational speed is doubled, NPSHR increases by four.

## Rotary Pumps

Rotary pumps use gears, lobes, screws, vanes, or peristaltic action to facilitate rotary pumping action. They can be designed to pump liquids, gases, or mixtures of the two. As before, capacity per rotation is independent of driven speed. Contrary to reciprocal pumps, rotary pumps develop a dynamic liquid seal and do not require inlet and discharge check valves. Since the rotating element of the pump is directly connected to its driver via a shaft, some sort of drive shaft sealing arrangement is required. This is usually accomplished via a stuffing box, lip seal, or a mechanical seal. All rotary pumps undergo three rotational

conditions: OTI/CTO (open to inlet / closed to outlet), CTIO (closed to inlet and outlet), and OTO/CTI (open to outlet / closed to inlet).

**Peristaltic pumps** are typically used for pumping clean or sterile fluids. A schematic design of a peristaltic pump is shown in Figure 1-12 (White, 2003).

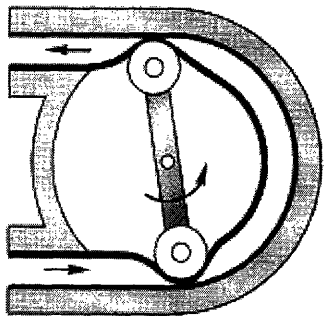

**Figure 1-12: Schematic design of a peristaltic pump**

**Vane pumps** consist of vanes mounted to a rotating rotor inside a circular cavity. The vanes slide in and out of the rotor, maintaining contact with the walls of the cavity. The centers of the rotor and the cavity are offset, so rotation occurs via eccentricity. A schematic design of a rotary vane pump is shown in Figure 1-13 (White, 2003).

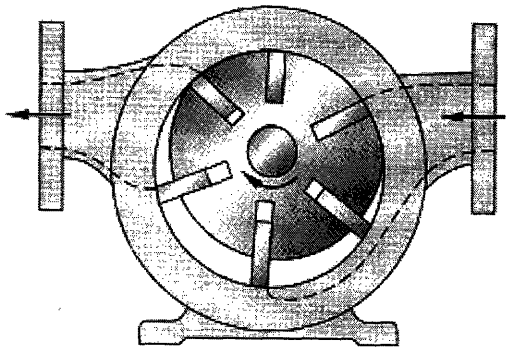

**Figure 1-13: Schematic design of a rotary vane pump**

**Gear pumps** use the revolving meshing of the gears to pump a fixed amount of fluid. Gear pumps can be designed to function as a motor or a pump. The two variations are external gear pumps (two external spur gears) and internal gear pumps (one external and one internal spur gear). When the gears separate at the intake side of the pump, the void creates a suction to pull in fluid. The fluid is carried as the gears rotate. At the discharge side of the pump, the gears mesh again to deposit the fluid. The clearances are on the order of micrometers to prevent the fluid from leaking backwards. The gears and housing have rigid designs to withstand high pressures and to pump highly viscous fluids. A schematic design of an external gear pump is shown below in Figure 1-14 (White, 2003).

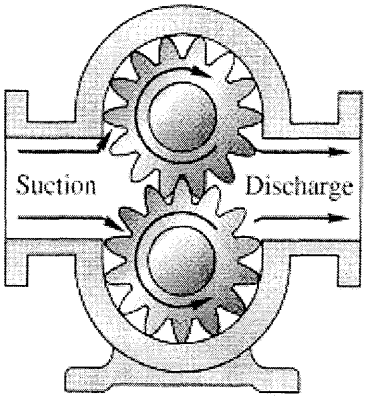


**Figure 1-14: Schematic design of an external gear pump**

**Lobe pumps** operate similarly to gear pumps, but without the lobes making contact. The lobes rotate out of mesh to create an expanding volume at the inlet of the pump. The fluid is trapped between the lobes and the interior casing as the lobes rotate. The fluid flows through the outlet port as the lobes mesh. Lobe pumps are typically used in food applications because they can handle solid particles. Since the lobes do not make metal-to-metal contact, the clearances do not need to be as tight as other positive displacement pumps (Dickenson, 1995). A schematic design of a three-lobe pump is shown in Figure 1-15 (White, 2003).

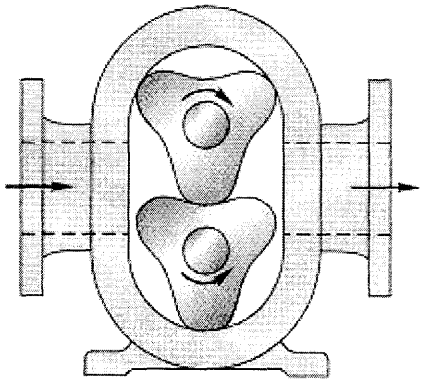

**Figure 1-15: Schematic design of a three-lobe pump**

**Screw pumps** have one or more screws to transfer fluids along an axis. Each screw thread carries a specific volume of fluid. Fluid transfer occurs by successive contact between the housing and the screw threads as the screw rotates (Dickenson, 1995). A schematic design of a double-screw pump is shown in Figure 1-16 (White, 2003).

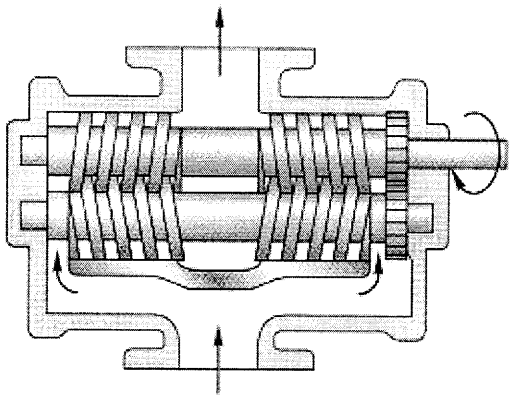

**Figure 1-16: Schematic design of a double-screw pump**

A **scroll pump** is also known as a scroll compressor or a scroll vacuum pump. Once the boiler pump efficiencies are determined, scroll pumps will be tested to measure their efficacy as an expander for the system.

For this project, the performance of automotive power steering pumps and a variety of OEM pumps are tested and compared. The most common power steering pump is the rotary vane pump. Power steering pumps supply pressure and thereby reduce steering efforts by the driver, making driving a more pleasant experience (Knowles, 2003). A typical steering assembly in a car includes pulleys, hoses, brackets, and steering boxes. A pulley is typically press-fit onto the pump's drive shaft; the pulley and shaft are then belt-driven by the engine. The diagram of the assembly of a power steering pump is shown in Figure 1-17 (Ciulla, 2003).

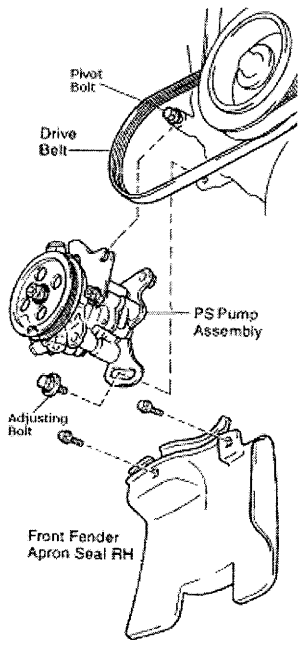


**Figure 1-17: Assembly of a power steering pump**

# Chapter 2 Experimental Set-Up

The test apparatus will help determine pump efficiency for various flow rates in different pressure regimes. The actual ORC unit will have the following properties: 2200kPa outlet, 207kPa inlet, 3LPM of 1.3kg/L HFC-245fa @30°C. The experiments for this study were initially performed using deionized water as the working fluid. It is more convenient to use water at ambient temperature as the working fluid instead of using the actual working fluid HFC-245fa when evaluating pump characteristics. HFC-245fa vaporizes at atmospheric pressure and temperature, making it difficult to work with for the pump performance tests. The data collected in the pump performance tests using the water-oil emulsion can be normalized, so it can be converted and used for predicting pump performance using HFC-245fa.

Initial experiments showed that deionized water caused the power steering pumps to stall, so 500 mL of WD-40 was added to 27 L of deionized water to fill the clearances in the positive displacement pumps and improve the volumetric efficiency. The lubricated emulsion had a measured density of 0.995 kg/L. This mixture was used for testing and determining performance curves for the pumps.

The primary thermodynamic variables of the fluid are its pressure, temperature, and density. Another important variable that characterizes a fluid's mechanical behavior is viscosity, a measure of a fluid's resistance to flow. The viscosity of the water-oil emulsion can be estimated using the Refutas equation (Maples, 2000).

(1) Calculate the Viscosity Blending Number (VBN) for each of the two components of the mixture, water and WD-40, using the following equation:

$$VBN_i = 14.534 \ln[\ln(v_i + 0.8)] + 10.975$$

where $v$ = kinematic viscosity in units of centistokes (cSt)

Since the kinematic viscosity of water, as found in literature, (White, 2003) is:

$$v_{water} = \frac{\mu}{\rho} = \frac{1x10^{-3}(kg/m \cdot s)}{998(kg/m^3)} = 1.01x10^{-6}\frac{m^2}{s} = 1.01cSt$$

$$VBN_{water} = 14.534 \ln[\ln(v_{water} + 0.8)] + 10.975 = 3.39$$

The kinematic viscosity of WD-40 is calculated from its density ρ and its dynamic viscosity μ (American Gas & Chemical Co. Ltd).

$$v_{WD-40} = \frac{\mu}{\rho} = \frac{0.005(kg/m \cdot s)}{802.8(kg/m^3)} = 6.23x10^{-6}\frac{m^2}{s} = 6.23cSt$$

$$VBN_{WD-40} = 14.534 \ln[\ln(v_{WD-40} + 0.8)] + 10.975 = 20.68$$

(2) Calculate the VBN for the blend using the mass fraction of each component, $x_i$.

$$VBN_{Blend} = [x_A * VBN_A] + [x_B * VBN_B] + ... + [x_n * VBN_n]$$

Since 500 mL of WD-40 was added to 27 L of water, the mass fractions are as follows:

$$x_{water} = \frac{m_{water}}{m_{total}} = \frac{(0.027m^3)(998kg/m^3)}{(0.027m^3)(998kg/m^3) + (0.0005m^3)(802.8kg/m^3)} = 0.985$$

$$x_{WD-40} = 0.015$$

$$VBN_{Blend} = [x_{water} * VBN_{water}] + [x_{WD-40} * VBN_{WD-40}] = 4.69$$

(3) Solve for the kinematic viscosity of the blend.

$$v_{Blend} = e\text{^}e[\frac{VBN_{BLend} - 10.975}{14.534}] - 0.8 = 1.11cSt = 1.11x10^{-6}\frac{m^2}{s}$$

The density of the water-WD40 mixture was measured as 0.995 kg/L. The dynamic viscosity of the mixture can be determined by multiplying kinematic viscosity and density.

$$\mu_{Blend} = (\rho v)_{Blend} = (995\frac{kg}{m^3})(1.11x10^{-6}\frac{m^2}{s}) = 0.001\frac{kg}{m \cdot s}$$

The kinematic viscosity of HFC-245fa (Soffientini, 2003) is:

$$\mu_{HFC,liquid} = 0.402\frac{kg}{m \cdot s}$$

$$\mu_{HFC,vapor} = 0.0103\frac{kg}{m \cdot s}$$

The kinematic viscosities of the different fluids are related:

$$\mu_{Blend} \approx \mu_{water} < \mu_{WD-40} < \mu_{HFC,vapor} < \mu_{HFC,liquid}$$

The kinematic viscosity of the water-WD40 blend, roughly the same as that of water; is a few magnitudes less than that of HFC-245fa. The density of the water-WD40 mix is approximately equal to those of water, which is twice the density of HFC-245fa. Dimensionless parameters are useful in predicting the behavior of one fluid based on experimental data collected for a different fluid. In this case, dimensionless parameters obtained from using the water-WD40 mixture will be helpful in characterizing the behavior of HFC-245fa in a pump.

Fluid flow through pipes can be predicted using the Reynolds number, a ratio of inertial forces to viscous forces.

$$\text{Re} = \frac{\rho VL}{\mu} = \frac{VL}{v}$$

In *Fluid Mechanics*, White outlined how to analyze centrifugal pump performance in dimensionless terms. The typical output variables of a pump are head $H$ and brake horsepower *bhp*. They are dependent upon discharge $Q$, impeller diameter $D$, shaft speed $n$, fluid density $\rho$, viscosity $\mu$, and surface roughness $\varepsilon$.

$$gH = f_1(Q, D, n, \rho, \mu, \varepsilon)$$
$$bhp = f_2(Q, D, n, \rho, \mu, \varepsilon)$$

Using dimensional analysis principles, three dimensionless pump parameters were developed:

$$\text{Capacity coefficient, } C_Q = \frac{Q}{nD^3}$$

$$\text{Head coefficient, } C_H = \frac{gH}{n^2 D^2}$$

$$\text{Power coefficient, } C_P = \frac{bhp}{\rho n^3 D^5}$$

As mentioned before in Section 1.5, centrifugal pump efficiencies are inversely affected by increasing fluid viscosities, but positive displacement pumps are not. Thus, though the viscosities of HFC-245fa and water-WD40 are different, it is expected that the pumps using HFC-245fa will perform closely to the performance of pumps using water-WD40.

The dimensionless parameters would more useful if the project called for comparing pumps without regards to cost. However, the main goal of this project is to characterize pump efficiencies relative to cost, which is best illustrated by using actual pump performance.

Ideally, engineers of thermodynamic systems use pump curves relating flow, speed, power and head to make design choices for specific systems. In practice, however, it is difficult to obtain this information. This is due in part to the fragmented relationships between auto manufacturers, OEM suppliers, and the separate firms that actually sub-contract the design work and the mass manufacture of the pumps. Tracing this information through the auto manufacturers is difficult because the information is considered proprietary, or because there is a disinclination to discuss technical aspects of automotive equipment for use in applications outside of the automotive industry.

Despite the obstacles alluded to above, this project aims to verify the applicability of power steering pumps for use as boiler feed pumps in an ORC system. If a suitable candidate is identified, the project aims to undertake the effort to obtain OEM pump curves for comparison with the bench test data. The logic operating here is that in many cases testing pumps requires less effort than tracking down the pump curve from the manufacturer. A total of ten positive displacement pumps were tested. Seven pumps were automotive power steering pumps purchased from a local junk yard for the price of $50 each. They are classified as rotary vane pumps. Three pumps were specified and purchased from OEMs: a piston pump and two plunger pumps.

## 2.1 Test Station Set-Up

Assembling the pump test program required preparing the pumps as well as building a test stand. Prior to testing, the pumps were soaked and washed in parts cleaner fluids, pulleys were removed from the pumps' shafts, spider couplings were bored out to fit each pump's shaft, and the inlet and outlet ports were tapped appropriately to adapt with hose connectors. The center of the motor shaft is 3.5 inches higher than its base. The pumps were mounted to ensure that their shafts were also at the same height. Pump mounting brackets were made out of angle aluminum to properly orient the pumps on the test stand.

The apparatus for pump performance curve testing is mounted on a tube steel frame with a Lexan shield for safety during pump tests. An aluminum platform supports two pressure vessels (38 L and 26 L capacities), a motor and a pump. Hoses, valves, flow meters, and pressure gauges. During testing, the pressure vessels are loaded with water and pressured using compressed air. Higher pressures are obtained in the high-side tank via the piston effect of water on the air headspace. The pressure in the low-side tank is maintained at 207 kPa, while the pressure in the high-side tank continually increases. Measurements are taken in increments of 69 kPa on the high-side pressure tank, starting at 552 kPa and ending at 2760 kPa. The pressure gauges read in units of psi, but for consistency sake, SI units are used throughout the text. A picture of the test apparatus is shown in Figure 2-1 below.

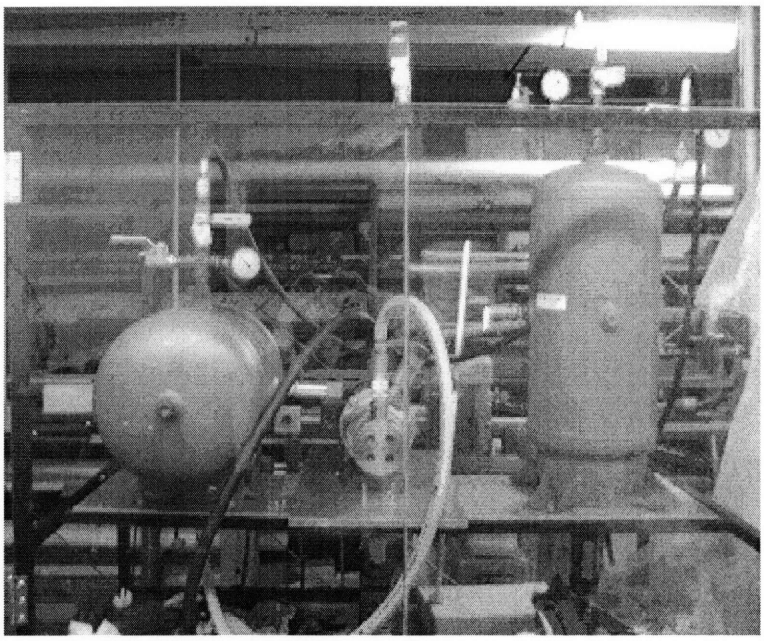

**Figure 2-1: Photograph of test apparatus**

### Motors

A Baldor 0.5 hp motor running at 1725 rpm is used only to run the Dynex plunger pump (Setup A). The remaining pumps are powered by a Leeson 1.5 hp variable speed controlled DC motor (Setup B). In Setup B, the motor speed can be varied from 0-1650 rpm. In Setup A, the motor shaft is directly coupled to the pump shaft via spider couplings. In Setup B,

the motor shaft is connected to a torque transducer, which is connected to the pump shaft; both connections are via spider couplings.

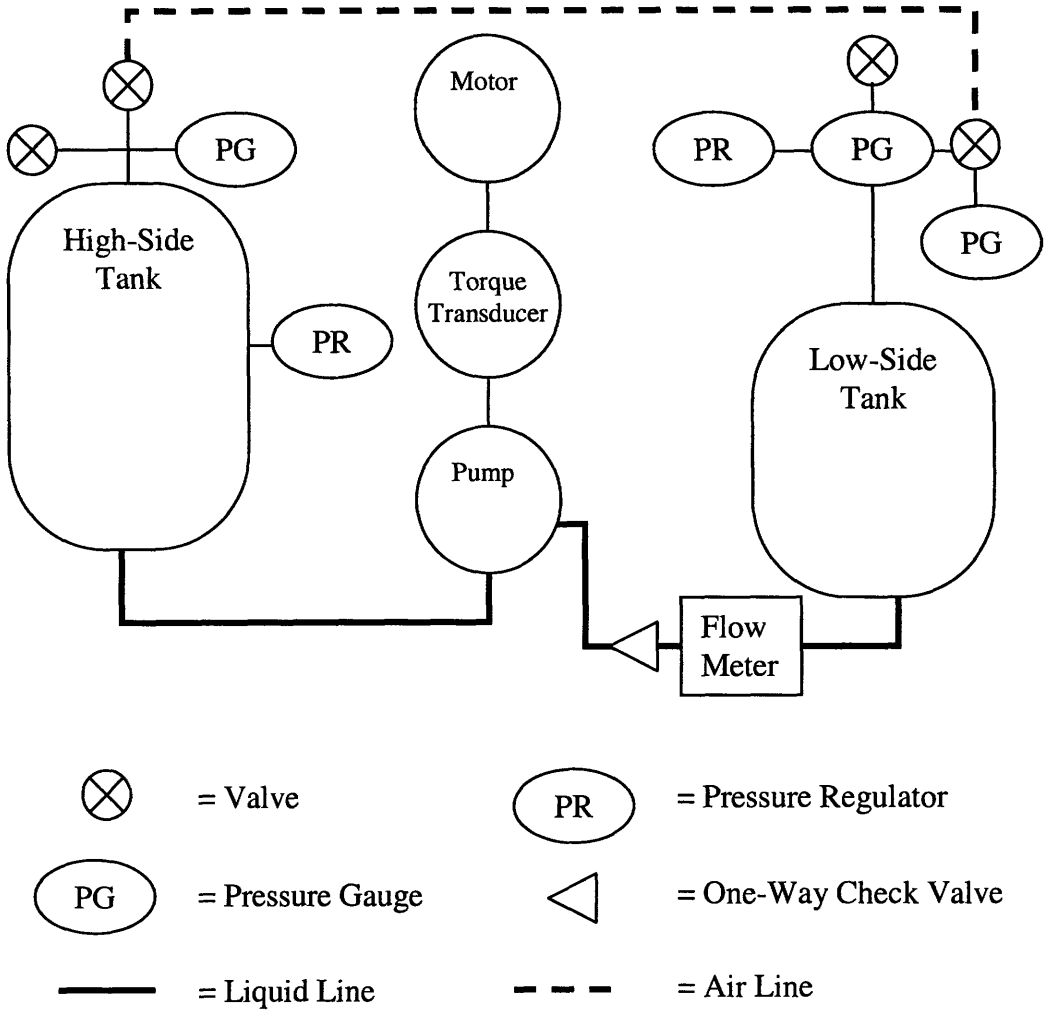


**Figure 2-2: Schematic of Test Apparatus Layout (Setup B with Torque Transducer)**

## Tanks

The low-side pressure vessel has a capacity of 26 liters. The high-side pressure vessel has a capacity of 38 liters. Each tank is equipped with sight glasses located at the halfway mark.

As shown in Figure 2-3, the low-side pressure tank is equipped with a pressure-relief valve, an air valve, a pressure gauge, a pressure regulator, a hose for liquid, and a hose for air. The line loading to the pump inlet contains a flow meter and a one-way check valve.

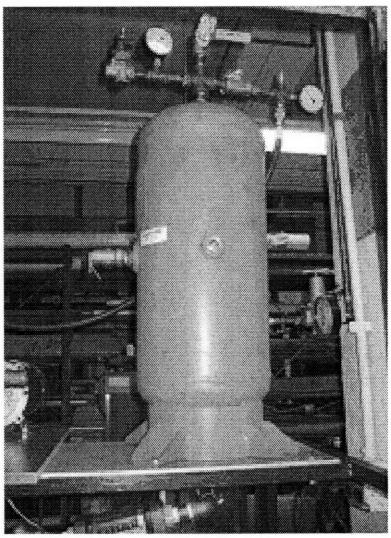

**Figure 2-3: Picture of low-side pressure tank**

The high-side pressure tank is equipped with a pressure-relief valve, an air valve, a pressure gauge, a pressure regulator, a liquid hose, and an air hose, as shown in Figure 2-4.

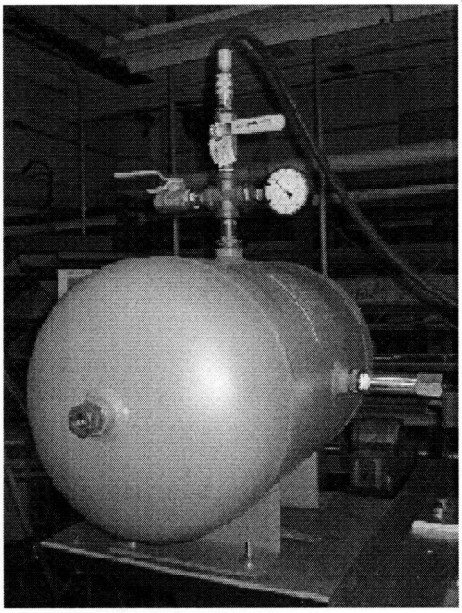

**Figure 2-4: Picture of high-side pressure tank**

## 2.2 Pump Measurement Apparatus

The test station can be modified to accommodate two different motor-pump configurations. A 0.5 hp 115VAC Baldor motor is used for testing the Dynex plunger pump. In this configuration, the motor and the pump are connected as one unit. A two pole switch is wired to the motor to function as a power on-off switch. Data are acquired visually, using a flow meter, pressure gauge, and a watt meter (P3 by Kill-A-Watt). The speed of the motor is fixed, so the pump's capacity is constant at 3.14 LPM.

A Leeson 190VDC motor is used for testing the rest of the pumps. In this configuration, the torque transducer is wired to a data acquisition unit (DATAQ Instruments). The motor voltage is set by a variable speed controller and the shaft output to the pump is via the torque transducer (Interface Instruments). The torque transducer is sensitive to vibrations caused by angular misalignment of the shafts. This requires careful alignment and the use of flexible spider couplings. The variable speed control allows the user to adjust the flow by varying the rotational speed of the pump. DATAQ records voltage measurements, corresponding to torque, which is then combined with the tachometer readings to calculate power consumption (Section 2.2.2). Additional data are acquired visually, using a flow meter, tachometer, and pressure gauge detailed below.

### 2.2.1 Equipment and User Interface

Noshok Pressure gauges are fixed to both the high-side and the low-side pressure vessels to display the pressures in the tanks, as shown in Figure 2-5 below.

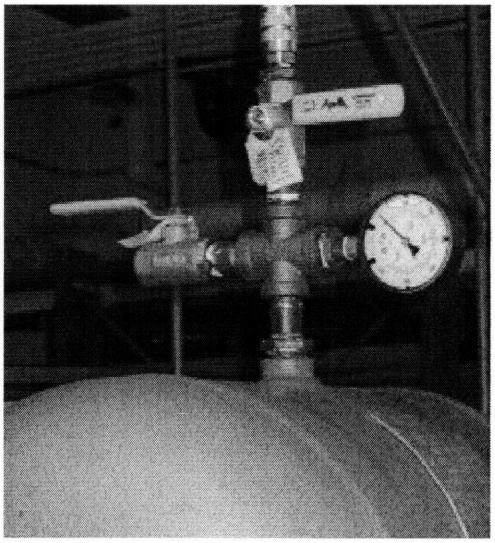

**Figure 2-5: Picture of pressure gauge (Noshok)**

A non-contact tachometer measures the rotational speed (rpm) of the motor. It is oriented such that the laser is directed at the reflective strip affixed to the spider coupling on the motor shaft, as shown in Figure 2-6 below.

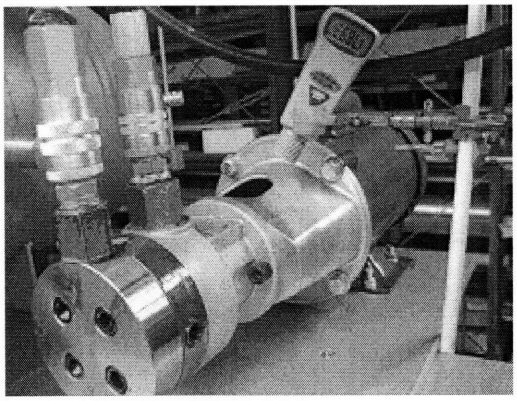

**Figure 2-6: Tachometer oriented toward the motor shaft of the Dynex pump (Setup A)**

A Hedland flow meter measures the flow rate (LPM) of the fluid as it is pumped from the low-side tank to the high-side tank. The unit used was factory calibrated for oil of specific gravity, $SG = 0.876$, and its nominal readout is in theory related to actual fluid flow by a connection factor:

$$\sqrt{\frac{0.876}{SG_{FlowingFluid}}}$$

The correction factor for the 0.995 SG water-WD40 fluid would be 0.938. However, tests indicated that the factor ranged from 0.9 to 1.0 (see Table 3-2). The flow meter is located between the two pressure vessels and is connected to a one-way check valve to prevent fluid flow from the high-side tank to the low-side tank, as shown in Figure 2-7 below.

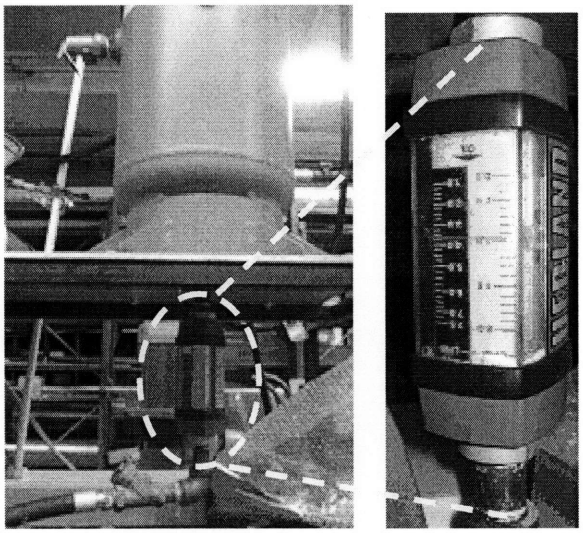

**Figure 2-7: picture of flow meter (Hedland)**

A P3 Kill-A-Watt meter measures the power (watts) consumed by the Baldor motor-Dynex plunger pump configuration (Setup A). The cord from the motor is plugged into the Kill-A-Watt meter, which is in turn plugged into a power strip containing a 15-Amp fuse, as shown in Figure 2-8 below.

**Figure 2-8: Picture of P3 Kill-A-Watt meter**

A variable resistance strain gauge bridge torque transducer derives torque from shaft torsion. The transducer accepts an 18V input and outputs a 0 to +5 voltage corresponding linearly to a 0 to 20Nm torque. The torque transducer is mounted on a flexible base with input and output shafts connected between the motor and the pump via spider couplings, as shown in Figure 2-9 below.

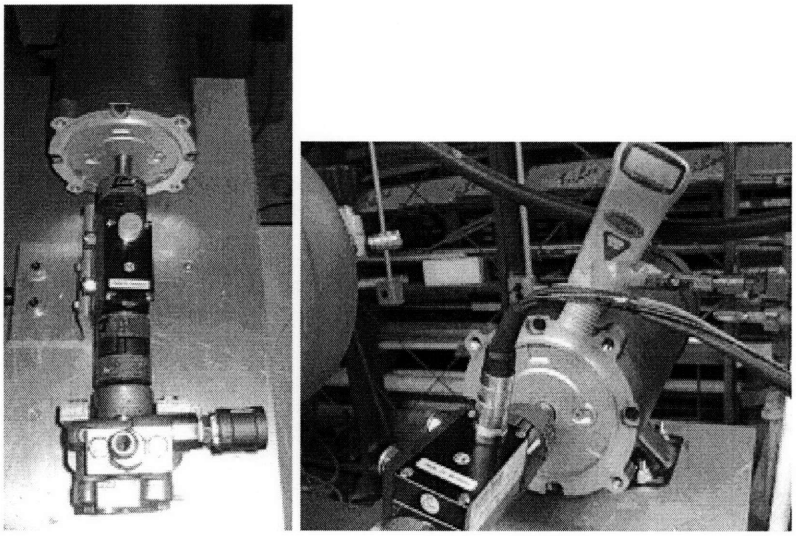

**Figure 2-9: Top View of the motor-torque transducer-pump configuration**

DATAQ consists of a data acquisition I/O unit that converts the analog signal from the torque transducer into a digital waveform and a software package that displays and records the digital waveform. A picture of the data acquisition unit is shown below in Figure 2-10.


**Figure 2-10: Picture of the DATAQ acquisition unit**

The user interface, showing voltage data from the DATAQ, is shown below in Figure 2-11.

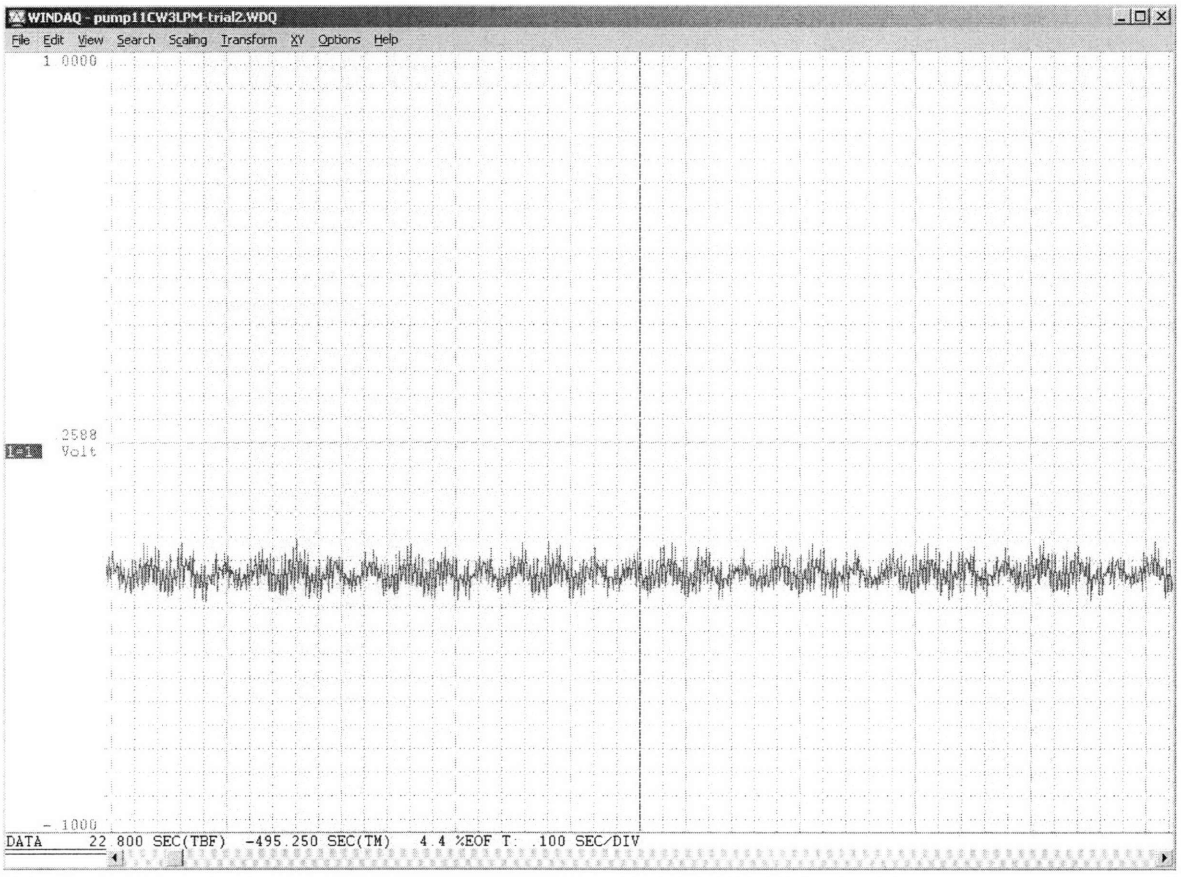


**Figure 2-11: Screenshot of the DATAQ software**

### 2.2.2 Operating Principles

The fundamental parameters used to assess pump performance are capacity, head, and input power requirements. Capacity describes the volume of fluid handled through the pump in unit time. The unit used in this project is liters per minute (LPM). Head describes the pressure developed on the fluid. The unit used in this project is meters (m). Head and pressure are directly related; head is independent of the cross section of the liquid column whereas pressure is the force per unit area. Head (H) and pressure (P) are related by the specific weight of the fluid (w):

$$P = wH$$

To describe any liquid, the equation is:

$P(bar) = 0.1 * H(meters) * SG$, where $SG$ is the specific gravity of the fluid.

The water (hydraulic) horsepower, the equivalent power output of a pump, can be measured by pressure and flow.

$$HP(output) = \frac{Q * H * SG_{fluid}}{K}$$

Q is the flow rate; H is the total head developed; K is a constant that depends on the units. For Q (GPM) and H (ft), K=33.

Alternatively, HP can also be represented using flow rate and pressure, as shown below.

$$WHP = \frac{Q(GPM) * P(psi)}{1714}$$

In metric units, the equation for the actual power consumed by the motor becomes:

$$Power_{Actual}(Watts) = \frac{Torque(Nm) * 2 * \pi * Speed(RPM)}{60}$$

The calibration of DATAQ is 20 Newton-meters per 5 Volts. Thus, torque is the voltage read by DATAQ times a factor of 4.

The brake horsepower *bhp*, the power required to drive a pump at a particular flow and head, is proportional to pressure and capacity. It can be measured by torque and speed. The equation for the input horsepower required at the pump shaft is:

$$HP(input) = \frac{Q(GPM) * P(psi)}{1714 * \eta}$$

In metric units, the equation for theoretical power consumed by the motor becomes:

$$Power_{Theoretical}(Watts) = H(meters) * FlowRate(kg/s) * 9.8(m/s^2)$$

Since the fluid used in these experiments is water, the conversion from volumetric flow rate (LPM) into mass flow rate (kg/s) is:

$$MassFlowRate(kg/s) = \left(\frac{Liters}{Min}\right)\left(\frac{\min}{60\sec}\right)\left(\frac{0.001m^3}{liter}\right)\left(\frac{1000kg}{m^3}\right)$$

The pump efficiency is defined as the theoretical power consumed divided by the actual power consumed by the pump:

$$\eta_{pump} = \frac{Power_{theoretical}}{Power_{actual}}$$

$$\eta_{pump} = \frac{\Delta P * Q}{MotorPower}$$

The overall ORC electrical system efficiency is defined as

$$\eta_{ORCsystem} = \frac{W_{electrical,net}}{Q_{in}}$$

It is a function of component (boiler feed pump and expander) efficiencies and is calculated using a MathCad tool developed by STG (STG Mathcad model, 2008).

Prior to installing a pump into the ORC system, it is imperative to have an understanding of pump performance curves. The simplest pump curve shows pressure versus flow. Additional factors for selecting a pump are pump efficiency, horsepower, and net positive suction head *NPSH* (Warring, 1984).

At a head difference of 203 meters, the ORC system power output as a function of pump efficiency, calculated using STG's MathCad model, is shown in Figure 2-12.

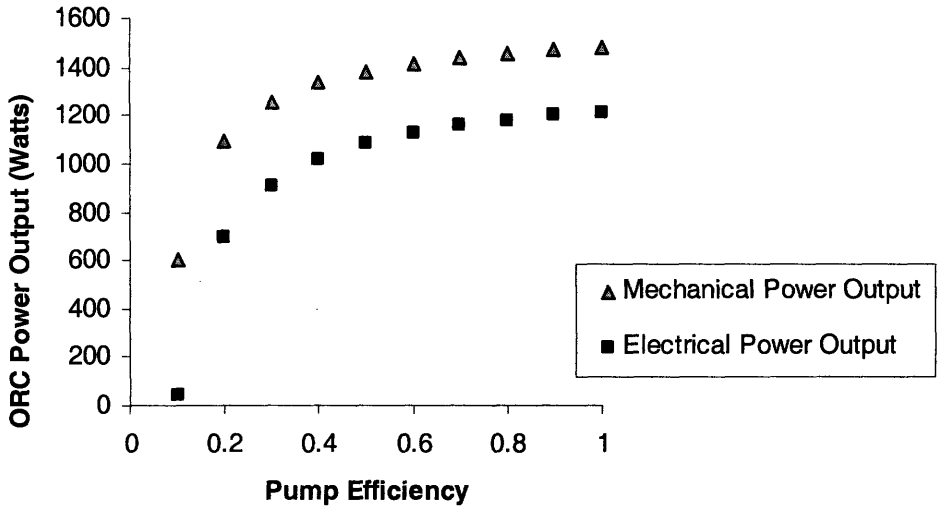


**Figure 2-12: ORC System Power Output vs Pump Efficiency**

The ORC system efficiency is defined as work out (mechanical and electrical) divided by heat into the system. The ORC system efficiency as a function of pump efficiency, calculated using STG's Mathcad model, is shown in Figure 2-13 below:

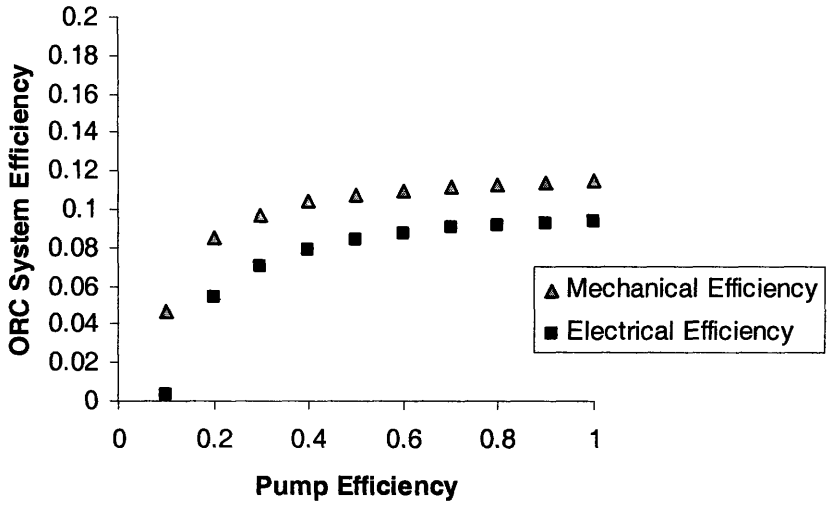


**Figure 2-13: ORC Cycle Efficiency versus Theoretical Pump Efficiency**

The assumptions for the inputs are displayed in Table 2-1 below (STG's Mathcad file, 2008).

**Table 2-1: MathCad Model Inputs**

| | |
|---|---|
| Mass Flow HFC-245fa | 0.065 kg/s |
| Boiler Outlet Pressure | 2206 kPa |
| Boiler Pressure Loss | 20 Pa |
| Psat(350 K) | 729 kPa |
| Turbine Isentropic Efficiencies | 0.5 |

A schematic of STG's organic Rankine cycle is shown below in Figure 2-14.

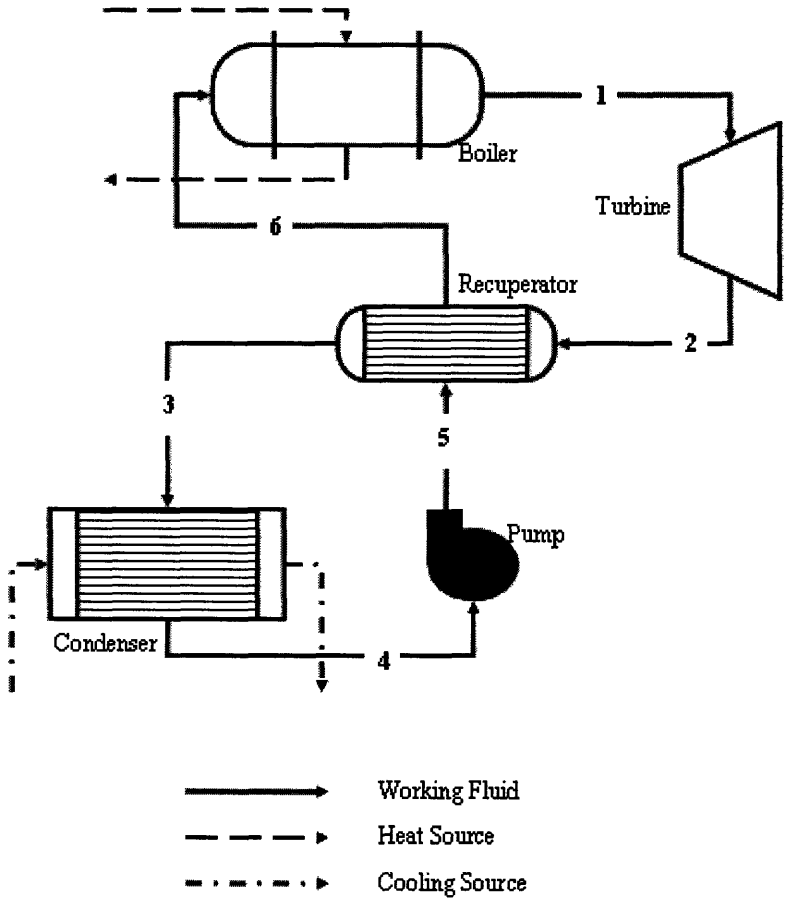


**Figure 2-14: Rankine Cycle. Adapted from STG's Mathcad model.**

The corresponding temperature-entropy (T-S) diagram for STG's ORC system is shown below in Figure 2-15.

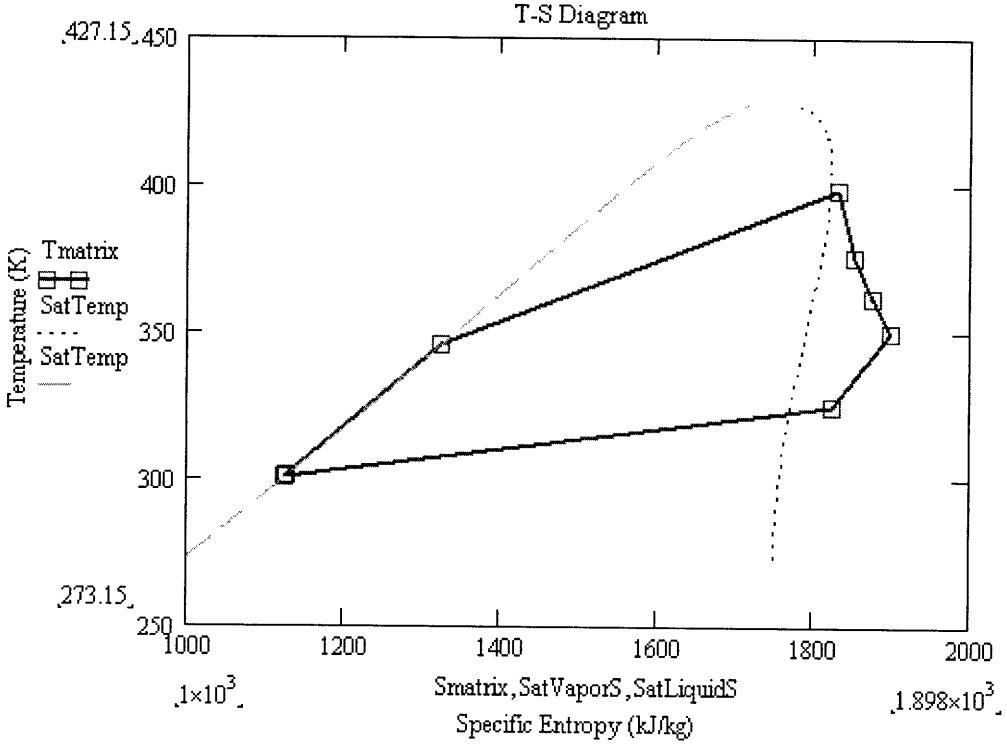


**Figure 2-15: Temperature-entropy (T-S) diagram for STG's ORC**

# Chapter 3 Pump Performance Study

## 3.1 Test Procedure

The low-side pressure tank is filled and the high side tank is partially filled (less than halfway) with water before either of the tanks is pressurized with air. The high-side pressure tank is first pressurized with compressed air to 345 kPa, the limit imposed by the compressor supply. Once pressurized the high pressure tank is isolated from the air supply with a ball valve. Next the air supply is routed into the low side tank via a ball valve, and pumping commences. The liquid flow is regulated by controlling the pump's rpms, and the back pressure on the pump suction is manually regulated to a pressure of 207 kPa. Pressure begins to increase in the high-side tank via the piston effect of water on the air headspace. The following measurements are taken in increments of 69 kPa on the high-side pressure tank, starting at 552 kPa and ending at 2760 kPa:

- Rotational speed of pump (tachometer, rpm)
- Fluid flow rate (flow meter, LPM)
- Power consumed (power meter, Watts)

**Dynex Pump**

The Dynex Pump is connected to the motor. The procedure to test it is as follows. Pressurize the tanks in the prescribed fashion. Turn on the motor using the light switch wired to the motor. Note the high-side tank pressure, the motor speed, the flow rate, and the power consumed.

**Automotive Power Steering Pumps and Two OEM Pumps**

The pumps are connected to the motor via a torque transducer. The torque transducer is connected to a data acquisition unit (DATAQ). The Leeson motor is connected to a variable speed control box; the motor speed is adjustable to control the flow rate.

The pumps using the Leeson motor are tested in clockwise (CW) rotations to generate "Efficiency versus Head" curves at flow rates ranging from 2 to 6 LPM. Many of the pumps did not flow at high enough rates in the counter-clockwise (CCW) configuration for the flow meter to register a reading.

**Table 3-1: Summary of metrics tested**

| High-Side Tank Pressure (kPa) | Nominal Flow Rate (LPM) | Rotation Direction |
|---|---|---|
| 552-2760 | 2, 3, 4, 6 | CW and CCW |

## 3.2 Analysis

The difference in pressure between the high-side and the low-side tanks is converted to head units of meters. The pressures discussed in this experiment are gauge pressures, whereas the pressures input into the thermodynamic ORC model are absolute; the pump data is graphically normalized to head so that the relevant design point can be easily extracted from the experimental data to the model input. The pump efficiency is the power out (conveyed to the fluid) divided by the power in (added to the pump), which is calculated from the torque transducer and tachometer measurements.

A calibration test on the flow meter showed that the specific gravity correction was inaccurate. The real flow rate was measured by setting the flow meter using the motor speed control, and timing with a stopwatch to see long it took to pump fluid into a measuring bucket. Flow rate data were corrected to reflect the real flow rate, displayed below in Table 3-2.

**Table 3-2: Flow Rate**

| Flow Meter Reading (LPM) | Actual Flow Rate (LPM) | Percent Error (%) |
|---|---|---|
| 2 | 2 | 0 |
| 3 | 2.85 | 5 |
| 4 | 3.63 | 10 |
| 6 | 5.21 | 15 |

**Evaluating Uncertainty**

In order to assess the accuracy of the results presented below, it is necessary to analyze the sources of uncertainties. The error in a measurement is the difference between the true value and the measured value, and is a sum of the bias error and random error. In general, experiments that are repeated many times generate a normal distribution, from which a statistical measure of uncertainty can be obtained. The notation is as follows:

$$result = mean \pm 2\sigma$$

Due to time constraints, the data collected in the pump performance experiments were not repeated enough times to obtain a normal distribution. Using the "constant odds" combination to combine the uncertainties due to $n$ independent variables, the formula is:

$$W_B = \sqrt{\left[\frac{\partial B}{\partial v_1} W_1\right]^2 + \left[\frac{\partial B}{\partial v_2} W_2\right]^2 + \cdots + \left[\frac{\partial B}{\partial v_n} W_n\right]^2}$$

where

$B$ = result

$W$ = uncertainty

$v$ = input variables

The instrumental uncertainty for the theoretical power consumed by the pump is described by the equation:

$$W_{TheoreticalPower} = \sqrt{\left[\frac{\partial TheoreticalPower}{\partial v_{Pressure}} W_{Pressure}\right]^2 + \left[\frac{\partial TheoreticalPower}{\partial v_{Flow}} W_{Flow}\right]^2}$$

Likewise, the instrumental uncertainty for the actual power consumed by the pump is described by the equation:

$$W_{ActualPower} = \sqrt{\left[\frac{\partial ActualPower}{\partial v_{Speed}} W_{Speed}\right]^2 + \left[\frac{\partial ActualPower}{\partial v_{Torque}} W_{Torque}\right]^2}$$

Thus, the uncertainty for pump efficiency is described by the formula:

$$W_{Efficiency} = \eta_{pump} \sqrt{\left[\frac{W_{TheoreticalPower}}{TheoreticalPower}\right]^2 + \left[\frac{W_{ActualPower}}{ActualPower}\right]^2}$$

The uncertainties are plotted as error bars in the graphs shown in the Appendix.

The quantifiable instrumental error sources, which are used to propagate uncertainties, are summarized below in Table 3-3.

**Table 3-3: Instrumental Uncertainties**

| Instrument | Uncertainty |
|---|---|
| Torque transducer (Interface, Inc) | ± 25 mV |
| Flow meter (Hedland) | ± 0.15 LPM |
| Pressure Gauges (Noshok) | ± 41 kPa |
| Tachometer | ± 0.04 rpm |
| Power Meter (Kill-A-Watt) | 0.2% |

The error bars on the graphs in the Appendix display uncertainties associated with instrumental errors. However, these errors do not account for human reaction variance e.g. resulting from manually synchronizing instrument observations with the timestamp of the DATAQ system. Furthermore, there could have been errors in assuming that that the DATAQ voltage waveforms for calculating torque were symmetrical about the median. Given more time, additional trials would have been conducted and the data averaged to determine the experimental error spread.

Two replicates were made of the Hypro Piston pump with the emulsified water at 2.85 LPM, and the efficiency vs. head curves were similar, as shown in Figure 3-1:

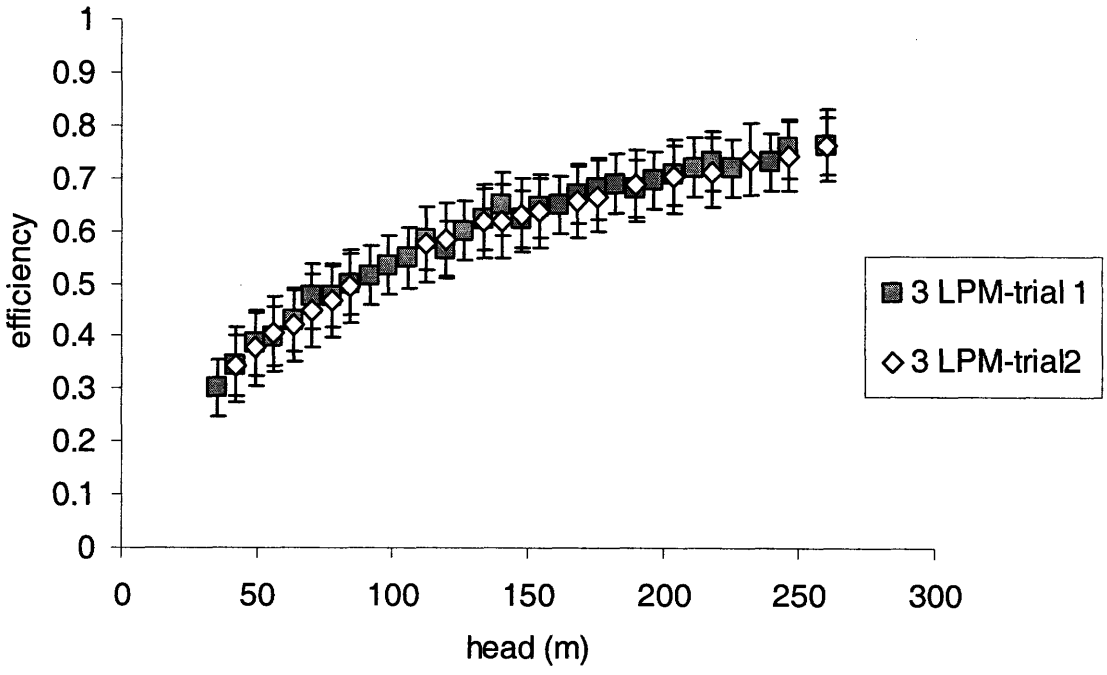


**Figure 3-1: Efficiency vs Head curve for HyproPiston Pump**

For simplicity's sake and in an effort to maintain the same environment and working conditions for each test, deionized water was initially used as the testing fluid. However, many of the power steering pumps' shafts seized after a few trials.

The power steering pumps operated at such low efficiency that they required higher torque than was available from the Leeson motor at high pressures. After adding some WD-40 to the water in the pressure vessels, the power steering pumps' efficiencies improved drastically, revealing that sufficient lubricity of the fluid is necessary for rotary vane pumps to operate.

## 3.3 Results

Rather than generating full pump performance curves, the purpose of this project was to characterize pump efficiencies based on specific head differentials. Thus, each pump has several "Efficiency vs Head" curves, measured at different flow rates, rather than "Head vs Capacity" curves.

Three of the pumps experienced shaft seals failure during the experiments and are not included in the results summarized below. The data, unless noted with "H2O" to represent water-only trials, are shown for trials using the lubricated water-WD40 mixture. The efficiency data displayed for the OEM Dynex pump (Setup A), a specialty pump made for pumping hydroflurorcarbons (HFC), include pump and motor efficiencies at a fixed flow rate of 3.14 LPM. Details of the results, with error bars for instrumental uncertainties, are shown in the Appendix.

A summary of the results at a nominal and actual flow rate of 2 LPM are shown below in Figure 3-2.

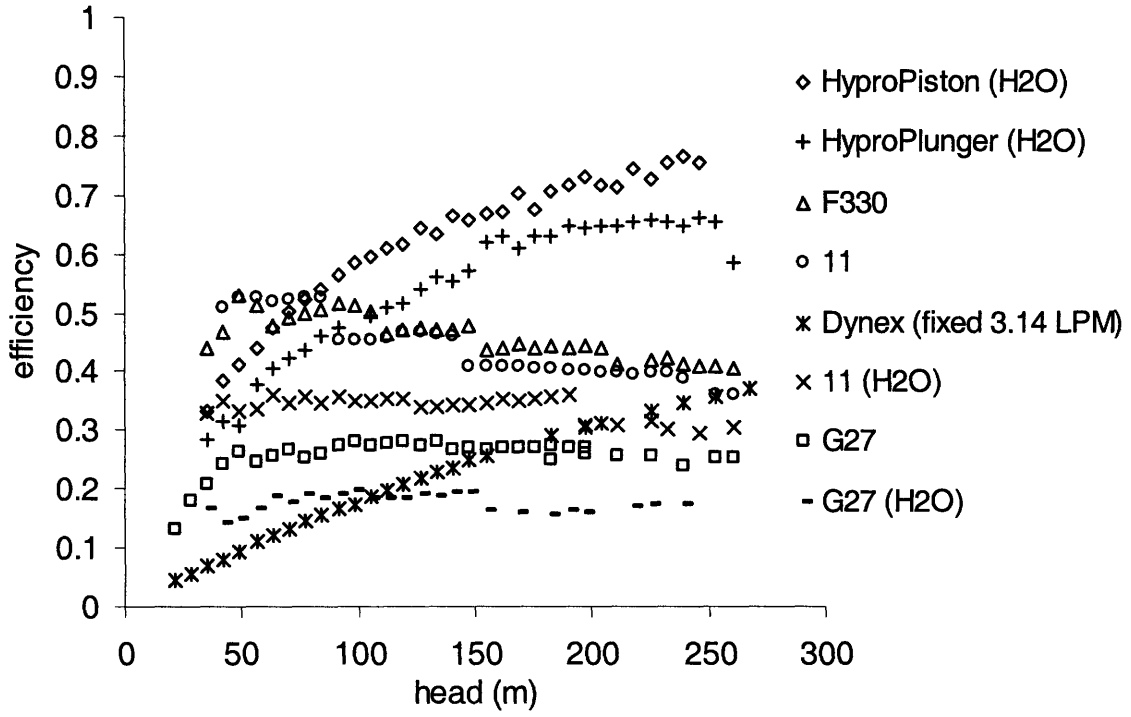


**Figure 3-2: Efficiency vs Head curves at a flow rate of 2 LPM**

A summary of the results at nominal flow rates of 3 LPM (2.85 LPM actual) are shown below in Figure 3-3.

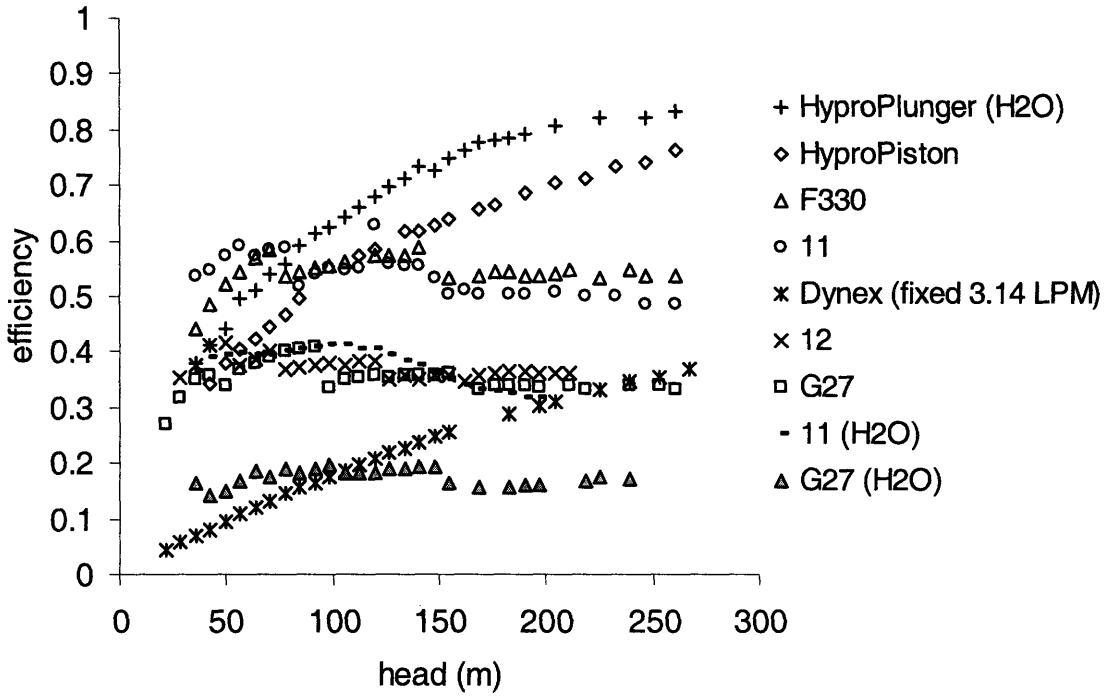


**Figure 3-3: Efficiency vs Head curves at a nominal flow rate of 3 LPM (2.85 LPM actual)**

A summary of the results at a nominal flow rate of 4 LPM (3.63 LPM actual) are shown below in Figure 3-4.

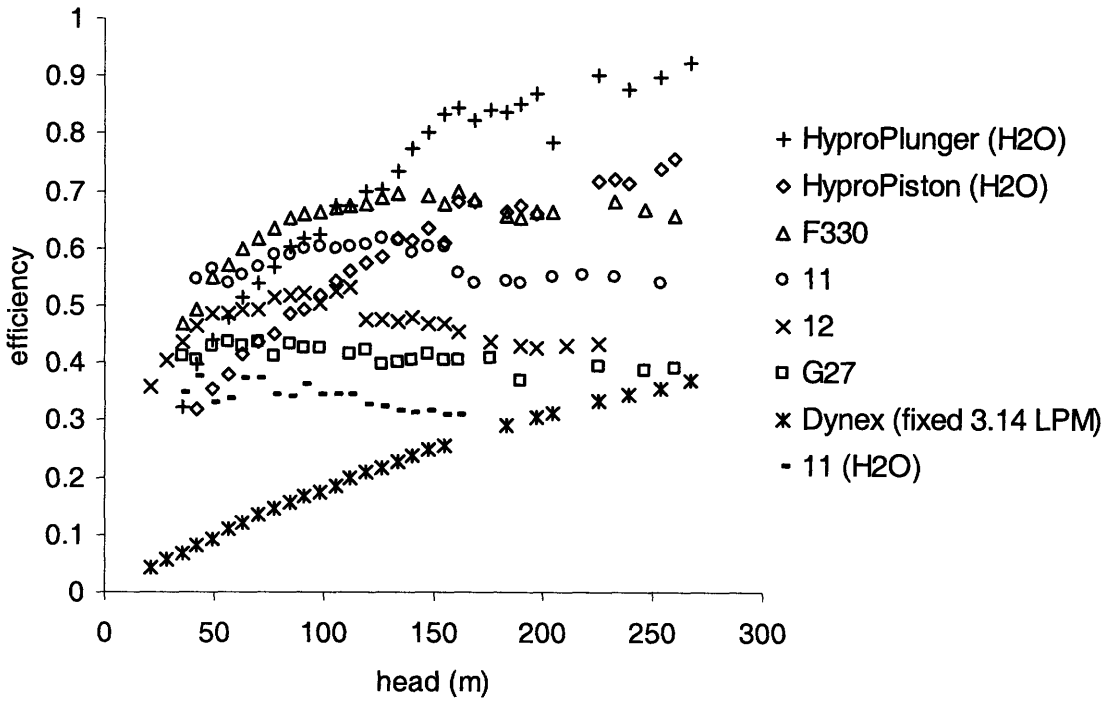


**Figure 3-4: Efficiency vs Head curves at a nominal flow rate of 4 LPM (3.63 LPM actual)**

A summary of the results at a nominal flow rate of 6 LPM (5.21 LPM actual) are shown below in Figure 3-5.

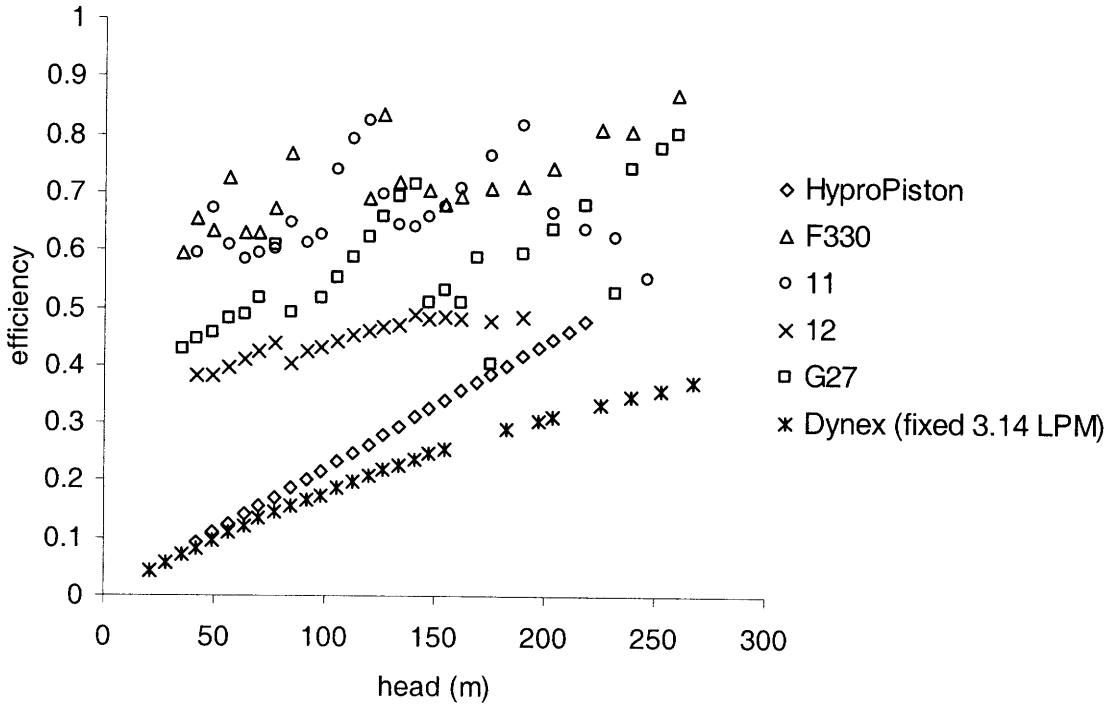


**Figure 3-5: Efficiency vs Head curves at a nominal flow rate of 6 LPM (5.21 LPM actual)**

The ORC system that STG is building has been designed around a specification of 3 LPM flow rate in order to achieve around 1 kW of electric power. Boiler feed pump efficiency influences the ORC system efficiency and determines the net electric work produced. Using operating conditions of 203 m head difference, 2.85 LPM flow rate and lubricated water, the results for pump efficiency, system efficiency and the net electric work output are shown below in Table 3-4.

**Table 3-4: Pump Efficiency, System Efficiency and Net Electric Work using operating conditions of 3 LPM flow rate and 203 m head difference**

| Pump ID | Pump Efficiency | ORC System Efficiency | Net Electric Work (kW) |
|---|---|---|---|
| HyproPlunger | 81% | 9.2% | 1.182 |
| HyproPiston | 70% | 9.0% | 1.156 |
| F330 | 54% | 8.5% | 1.101 |
| 11 | 51% | 8.4% | 1.087 |
| 12 | 36% | 7.6% | 0.980 |
| G27 | 34% | 7.4% | 0.959 |
| Dynex | 31% | 7.1% | 0.922 |
| GM | | NA - shaft seal broke | |
| ZF | | NA - shaft seal broke | |
| U02 | | NA – shaft seized | |

The optimal pump is selected based on: cost of the pump, total cost of the system, system efficiency, and the net electric work output. STG predicts that the solar electric power system will cost around $5000 ($2500 for the troughs and $2500 for the ORC unit), not including the cost of the boiler feed pump (STG, 2008). The power steering (PS) pumps were obtained from the junk yard at $50 each. The OEM pumps were more expensive. The HyproPiston and the HyproPlunger pumps were obtained from McMaster-Carr for $290.22 and $470.43, respectively. The Dynex pump cost $1200 with the motor and is predicted to cost $900 without the motor. The cost per watt was determined using the total cost of the system ($5000 + cost of pump) divided by the net work output. The cost of the system (in $/Watt) is shown in Table 3-5:

**Table 3-5: Cost of the solar electric power system**

| Pump ID | Cost ($/Installed Watt) |
|---|---|
| HyproPiston (OEM) | 4.58 |
| F 330 (PS) | 4.59 |
| HyproPlunger (OEM) | 4.63 |
| 11 (PS) | 4.65 |
| 12 (PS) | 5.15 |
| G27 (PS) | 5.27 |
| Dynex (OEM) | 6.40 (without motor); 6.72 (with motor) |

The most suitable pump for STG's 1-kWe ORC system is the HyproPiston pump. Although the cost of the HyproPiston pump is nearly six times that of a junk yard power steering pump and the system efficiency is lower compared to that of the HyproPlunger pump, the HyproPiston has the lowest cost when normalized over the power output.

# Chapter 4 Discussion

In general terms, the design of a small scale Solar ORC depends on several variables, which can be controlled in the design process to a varying extent. The design must necessarily specify the size of the power output; in this case, a design output of 1-$kW_e$ is considered. The design variable most responsible for scaling the work output is the mass flow rate of the working fluid. Because cost of materials and components are externally fixed, there is usually an interest in maximizing efficiency and distributing power output over smaller capital costs. As Carnot noted, increased efficiency is mainly a result of increasing the temperature differential across the heat engine:

$$\eta_{Carnot} = 1 - \frac{T_{cold}}{T_{hot}}$$

Because the cold side temperature is typically limited by ambient temperatures on earth, increasing the temperature differential invariably means raising the high side temperature.

Other aspects of ORC design affecting efficiency include the head losses in the plumbing, the isentropic efficiency in the expander and pump, motor and generator efficiencies and parasitic losses (control systems, energy expended in delivering and rejecting heat). Efforts to increase efficiency usually involve tradeoffs, e.g. increasing the temperature of heat addition to a Solar ORC involves more expense to combat heat loss at the collectors and thermal fluid loop. Adding a recuperator will increase thermal efficiency but involves increased head losses and expense. However, as noted in Section 3.3, while the increase in cost of a component is added to the total system cost, the associated cycle efficiency increase is distributed across the total costs of the system which can result in a lower cost per watt.

Varying the temperature of heat addition directly varies the pressure ratio of the ORC, and the expander volumetric ratio (expansion ratio) must be matched accordingly. Because expanders for small scale Solar ORC applications are not widely available at present, STG has explored the potential for using commonly available HVAC scroll compressors as an expander. Because expansion ratio is a function of the scroll geometry, the expansion can only occur in discrete stages, which further constrains the operating temperature parameters.

The purpose of this study has been to examine the role of feed pump efficiency on overall ORC performance and cost-effectiveness. Because specialty boiler feed pumps are expensive (e.g. ~$1000), the possibility of adapting OEM pumps from other applications, namely general purpose pumps and automotive power steering pumps was evaluated.

Generally speaking the pump efficiencies at the ORC design point ranged from 25% to 75%. The relevance of these results to pump selection is discussed below.

The Dynex plunger pump, the most expensive pump, was designed specifically for pumping HFC-245fa at 3LPM with a 300psia outlet and 30psia suction. It flowed approximately 3LPM with a combined pump and motor efficiency of between 30 and 40% at the specified pressure ratio. This pump was intended to be the performance benchmark for the pumps adapted from other applications, however it underperformed many of them in terms of isentropic efficiency and was much more expensive than any other pump.

A number of the power steering pumps, obtained from junk yards for $50 each, also did not exhibit high efficiencies, and some pumps exhibited diminished efficiency pumping against higher pressures. It seems likely that the pumps were tested at flow rates below their designed optimal (typically 10-12 LPM in power steering systems). The amount of flow provided by power steering pumps depends on the engine speed and the pulley ratio between pump and crankshaft. An idle engine speed is approximately 1000 rpm, while an engine at full speed can exceed 6000 rpm. Most of the power steering pumps examined did not generate high power efficiencies at the desired flow regime of 3 LPM, and thus are not ideal for the size of the ORC being considered (1 $kW_e$). Some of the pumps performed reasonably well at 6LPM, indicating that for flow rates nearer their design points their efficiency could be become acceptable for use in larger ORCs (2-3 $kW_e$).

The Hypro piston and plunger pumps were designed to pump water and both exhibited high efficiencies relative to the power steering pumps. The HyproPiston is rated with a maximum flow rate of 5.7 LPM at 500psi (3447 kPa) and the HyproPlunger is rated with a maximum flow rate of 18 LPM at 2000psi (13,790 kPa). The "Efficiency vs Head" graph for the HyproPiston pump implies that the maximum pump efficiencies are obtained at half of the maximum flow rates. If this were true for all pumps being examined, then it would indicate that power steering pumps would have peak efficiencies at flow rates in the vicinity of 6 LPM.

Based on pump performance curves, an appropriately-sized motor and pulley ratio can be chosen to drive the pump at a reduced speed. For example, the electric motor can have a speed of 1725 rpm, but the pump can be driven at 950 rpm. The equation below can be used to size a pulley (Hypro Manual, 2006):

$$\frac{MotorRPM}{PumpRPM} = \frac{Flow(@\ RatedSpeed)}{Flow(Desired)} = \frac{PumpPulleyDiameter}{MotorPulleyDiameter}$$

Alternately, a speed reducer of the appropriate ratio can be interposed between the motor drive and pump. This is discussed in the Appendix.

Rural communities that do not have access to the electric grid, such STG's test sites in Lesotho, often use diesel engines to generate power. Diesel fuel has an energy content of 42.8 MJ/kg (lower heating value) and a density of 0.837 kg/L (US DOE, 2006). Diesel engines have electric conversion efficiencies of roughly 35% (Dickenson, 1995). In other words, one liter of diesel fuel would produce a power output of 12.5 MJ rather than the theoretical power output of 35.8 MJ. As mentioned before, pump and expander efficiencies affect the overall ORC system efficiency. Assuming an complete expansion and an

expander efficiency of 50%, a boiler feed pump efficiency of 70% (HyproPiston pump), and a head differential of 203 m, the ORC system power output is calculated to be 1.2 $kW_e$ and has a system efficiency of 9%. If the ORC system operates for ten hours a day and lasts ten years lifetime, it would generate 42 $MW_e$-hr, which is equivalent to a displacement of over 14,000 liters of diesel fuel and $3.5x10^4$ kg of $CO_2$.

A plot of the diesel fuel displaced as a function of a pump with 70% efficiency is shown below in Figure 4-1.

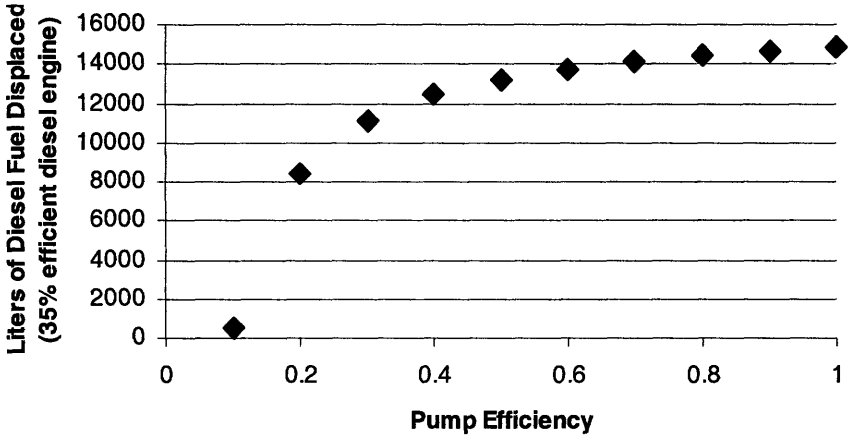


**Figure 4-1: Diesel Fuel Displaced (liters) vs Pump Efficiency**

A graph of amount of carbon dioxide displaced as a function of a pump with 70% efficiency is shown below in Figure 4-2.

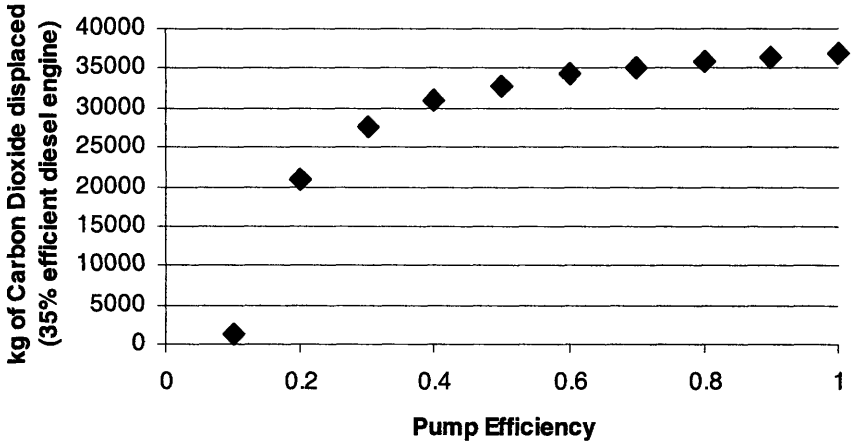


**Figure 4-2: Carbon Dioxide Displaced (kg) vs Pump Efficiency**

An inefficient pump, such as the Dynex with an efficiency of 30% at the parameters listed above, would displace a little over 11,000 liters of diesel fuel and $2.8x10^4$ kg of $CO_2$ over ten years.

The improvement in system efficiency can be summarized by calculating the difference in diesel fuel savings from picking an efficient boiler feed pump (70%) over picking an inefficient pump (31%) for the ORC. These savings scale proportionally with an increase in power output by the system. Thus, while the savings from building a 1-$kW_e$ system seem small, the savings are significant if 10, 100 or 1000 of these 1-$kW_e$ systems are built, or if a single system produces 10, 100 or 1000 times more power than a 1-$kW_e$ system. For a solar trough-ORC system that runs for 36,500 hours, the difference in the diesel fuel saved and in the amount of carbon dioxide displaced from picking a 70% efficient pump over a 30% efficient pump is tabulated in Table 4-1.

**Table 4-1: Difference in savings from picking 70% efficient pump rather than 30% efficient pump, as a scale of system power output**

| | 1 $kW_e$ | 10 $kW_e$ | 100 $kW_e$ | 1000 $kW_e$ |
|---|---|---|---|---|
| Liters of Diesel Fuel Saved | 2861 | 28,610 | 286,101 | 2,861,019 |
| kg of $CO_2$ offset | 7113 | 71,129 | 711,295 | 7,112,945 |

Carbon dioxide emissions from US power plants are roughly 1.7 Gt/year (Tester et al, 2005). Putting the numbers from Table 4-1 into context, over 239,000 1000-$kW_e$ solar trough-ORC systems would be necessary to offset annual carbon dioxide emissions from US power plants.

# Chapter 5 Conclusions

The goal of this study was to determine performance curves for a variety of positive displacement pumps in order to select an efficient and low cost option for use as a boiler feed pump in a 1-kW ORC system built by the Solar Turbine Group in Lesotho. Since boiler feed pump efficiency impacts the overall system performance of a small scale (1 $kW_e$) ORC, it is imperative to select an optimal and affordable pump. The optimal pump was selected based on how the pump efficiency affected the overall ORC system efficiency and the net electrical power output. This project demonstrates that pre-owned power steering pumps can produce efficiencies in the range of 34%-54% for the prescribed ORC operating conditions with water-oil emulsion as the working fluid. For that pump efficiency range, the overall ORC system efficiency would be 7.4%-8.5% and overall system cost would be USD $4.59-$5.27 per installed Watt. The OEM pump made by Dynex specifically for hydroflurocarbon applications had relatively poor performance. The pump efficiency was 31%, giving a system efficiency of 7.1% and a cost of USD $6.40 per installed Watt. The OEM water piston and plunger pumps made by Hypro achieved efficiencies of 70% and 81%, respectively under the same ORC operating conditions described above. For that pump efficiency range, the overall system efficiency would be 9.0% and 9.2% and cost would be USD $4.58 and $4.63 per installed Watt, respectively. Though the HyproPiston pump was nearly six times more expensive than the power steering pump options, the efficiency gains result in a lower cost per watt. The pump performance curves identified in this project will be used for matching with the parameters of the other crucial mechanical component in the ORC: the expander. Like the boiler feed pump, the expander performance affects the overall system efficiency. The next phase of research will experimentally evaluate the feasibility of using automotive scroll pumps as expanders in the Solar ORC unit.

# References


American Gas & Chemical Co. Ltd. "Comparison of TSI 301 & WD-40). http://www.tsi301.com/comparison.htm (27 Jan 2008).

Barber, R.E. and F. P. Boda. "Organic Rankine Power Conversion Subsystem Development for the Small Community Solar Thermal Power System." JPL Parabolic Dish Solar Thermal Power Ann. Program Rev., Proc, 1982: 101-113.

Ciulla, Vincent T. "1998 Toyota Camry 2.4 Liter Power Steering Pump Assembly." Auto Repair. 2003.
http://autorepair.about.com/library/images/bl637a-lib.htm (20 Dec 2007).

Dickenson, T.C. *Pumping Manual. 9th Edition.* New York: Elsevier Science Ltd, 1995.

Energy Information Administration (EIA). "Energy Kid's Page: Solar Energy." November 2007. http://www.eia.doe.gov/kids/energyfacts/sources/renewable/solar.html (10 December 2007)

Hypro. Powerline Plus 2000 Plunger Pumps. "Installation, Operation, Repair, and Parts Manual." 2006

Kane et al. "Small Hybrid Solar Power System." *Energy* 28 (2003): 1427-1443.

Knowles, Don. *Automotive Suspension and Steering Systems.* Clifton Park, NY : Thomson Delmar Learning, 2003: 244.

*Maples, Robert E. Petroleum Refinery Process Economics, 2nd Edition. Tulsa, OK: Pennwell Books, 2000.*

McMahan, Andrew. "Design and Optimization of Organic Rankine Cycle Solar-Thermal Power Plants." MS thesis, University of Wisconsin-Madison, 2006.

McMaster-Carr. http://www.mcmaster.com/. (15 Jan 2008).

McNally Institute. http://www.mcnallyinstitute.com/13-html/13-06.htm

NREL. "Parabolic Trough Power Plant System Technology." (10 April 2007) http://www.nrel.gov/csp/troughnet/power_plant_systems.html. (23 Jan 2008)

Personal Communication with STG. 12 Jan 2008.

Soffientini, Cesare, Gary J. Zyhowski, and Mark W. Spatz. "HFC-245fa: An Overview of Properties and Applications." Honeywell, 2003. www.centrogalileo.it/nuovaPA/Articoli%20tecnici/INGLESE%20CONVEGNO/HONEYWELLinglese.doc. (15 Jan 2008).

STG International. 2007. http://www.solarturbinegroup.org/ (12 Dec 2007)

STG's Mathcad file. "ORC Model." 2008.

Tester, J., et al. *Sustainable Energy: Choosing Among Options*. Cambridge, MA: MIT Press, 2005.

US Department of Energy: Hydrogen Analysis Resource Center. "Lower and Higher Heating Values of Hydrogen and Fuels." March 2006. www.hydrogen.pnl.gov/filedownloads/hydrogen/datasheets/lower_and_higher_heating_values.xls. (25 Jan 2008)

Volk, Michael. *Pump Characteristics and Applications: 2nd edition*. New York: CRC Press, Taylor & Francis Group, 2005.

Warring, R.H. *Pumps: Selection, Systems, and Applications. 2nd edition.* England: Trade & Technical Press Ltd, 1984.

White, Frank M. *Fluid Mechanics. Fifth Edition.* Boston: McGraw Hill, 2003.

Wu, Chih. *Thermodynamic Cycles: Computer-Aided Design and Optimization.* New York: Marcel Dekker, 2004.

# Appendix

Many of the power steering pumps were torque-limited by the Leeson motor, which is capable of exerting a maximum torque of 6 Nm across its range of speeds to a maximum of 1.5 hp. In other words, it will put out 6 Nm at 1 rpm and at 1700 rpm. Thus, in order to get more torque at lower speeds, it is necessary to reduce the speed of the motor. Using data from one of the power steering pumps, the graph shown below in Figure A. 1 was generated to determine what speed reduction ratio should be used. It accounts for pump efficiencies ranging from 10% to 25%. For future tests, a speed reduction by a factor of 2 should be sufficient to obtain desirable pump efficiencies.

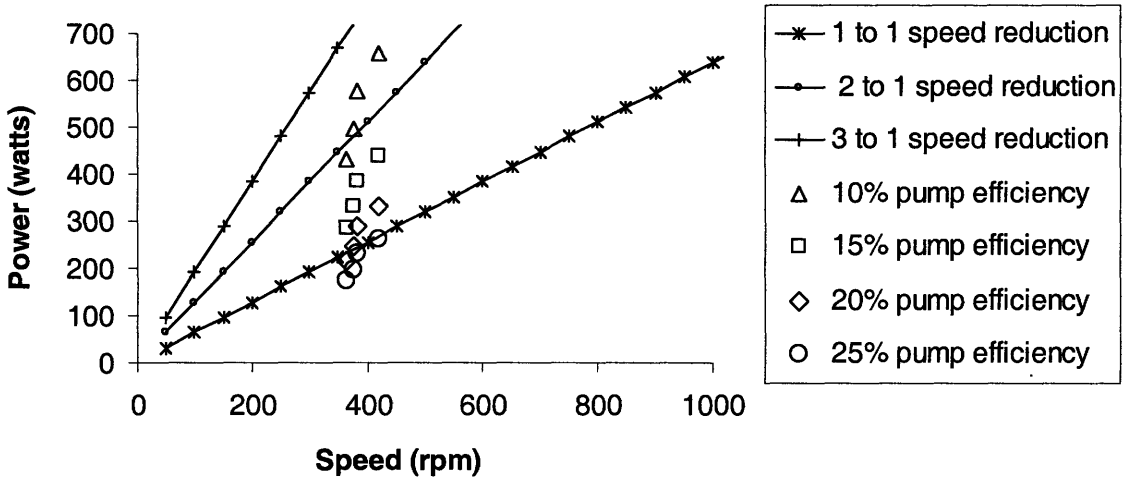


**Figure A. 1: "Power vs Speed" graph to determine speed reduction ratio for motor**

Each pump was tested at several different flow rates and its "Efficiency vs Head (m)" curves are shown below in Figure A. 2 through Figure A. 19. The flow rates are labeled as the nominal values, but the plots have been corrected for the actual flow rates. The pump efficiency was a measure of the theoretical power consumed divided by the actual power consumed. Unless otherwise noted, the working fluid used to generate the data below was a mixture of water-WD40. Data generated using deionized water as the working fluid is noted as "(H2O)" in the legend. All flow rates are listed as nominal values, except for the Dynex pump which is fixed at 3.14 LPM. The efficiencies plotted for the Dynex pump include the pump and motor efficiencies, since the motor and pump were combined (Setup A).

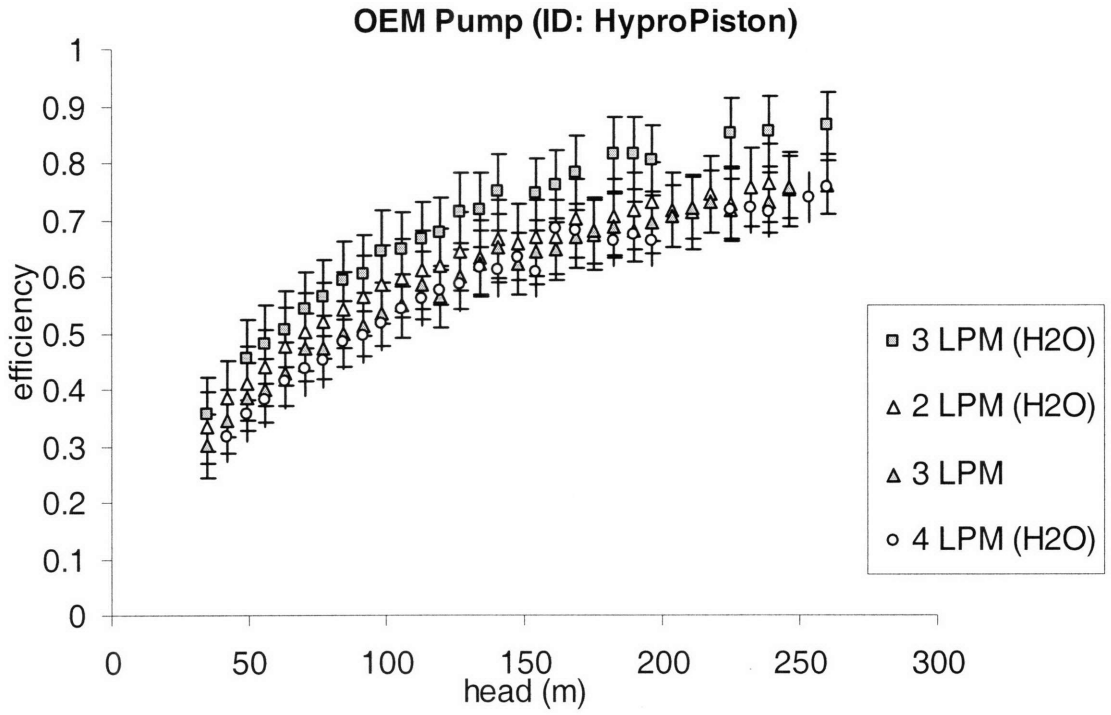


**Figure A. 2: HyproPiston pump performance curve**

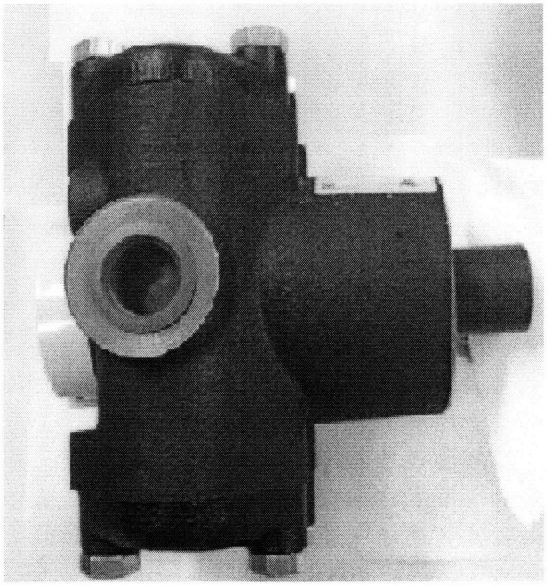

**Figure A. 3: Picture of HyproPiston pump**

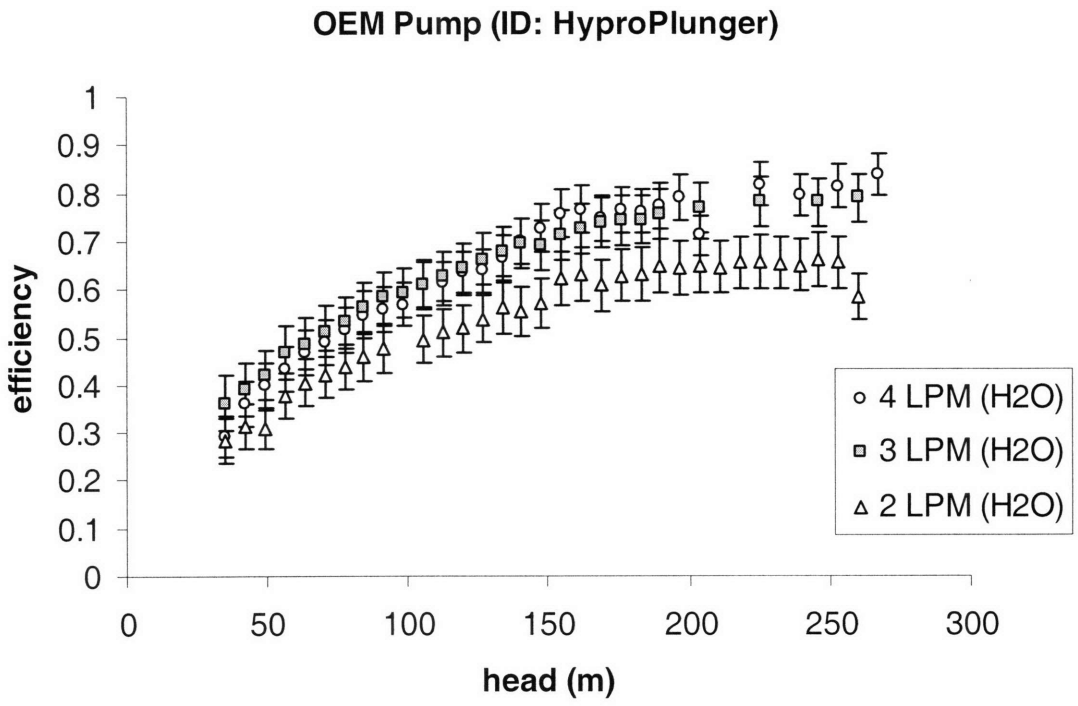


**Figure A. 4: HyproPlunger pump performance curve**

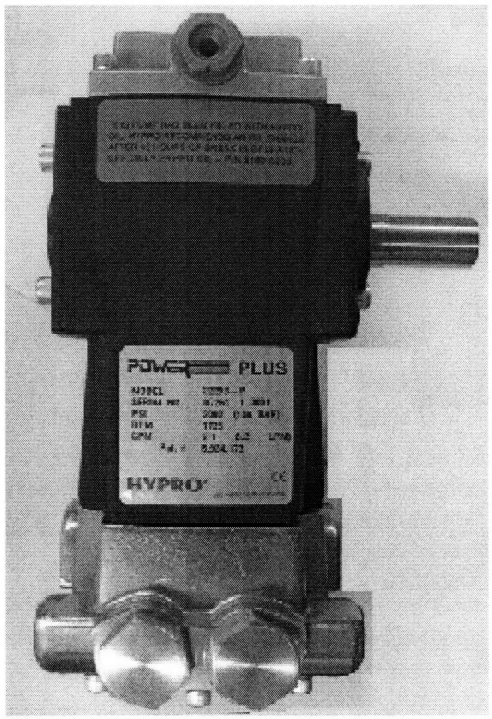


**Figure A. 5: Picture of HyproPlunger pump**

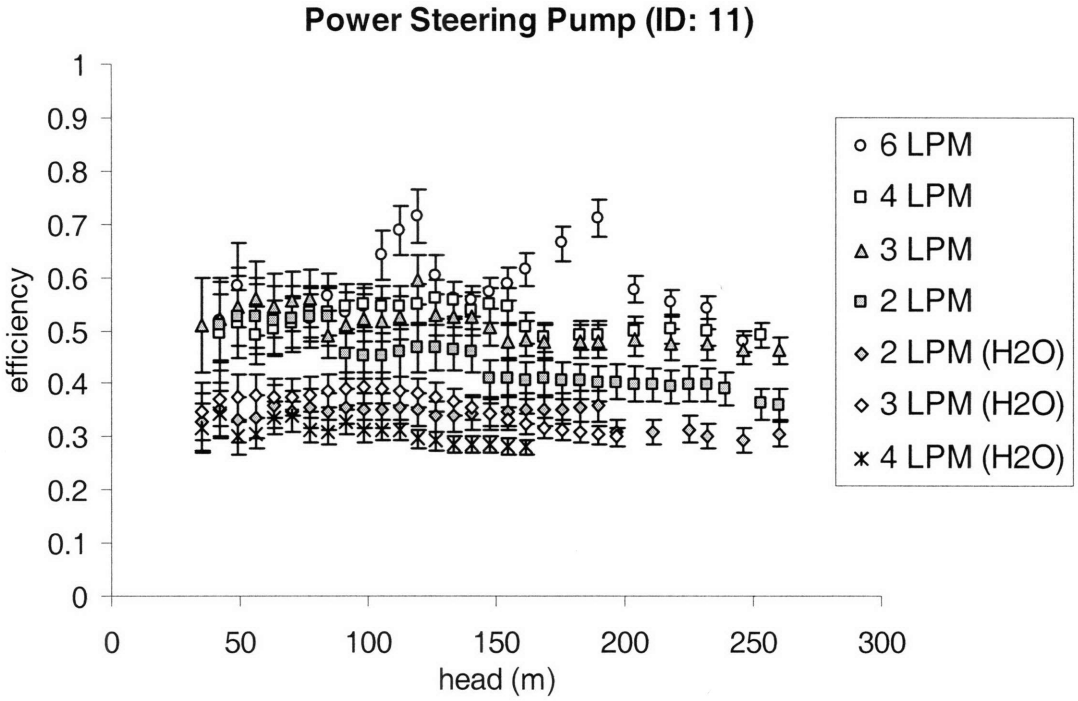


**Figure A. 6: Pump11 pump performance curve**

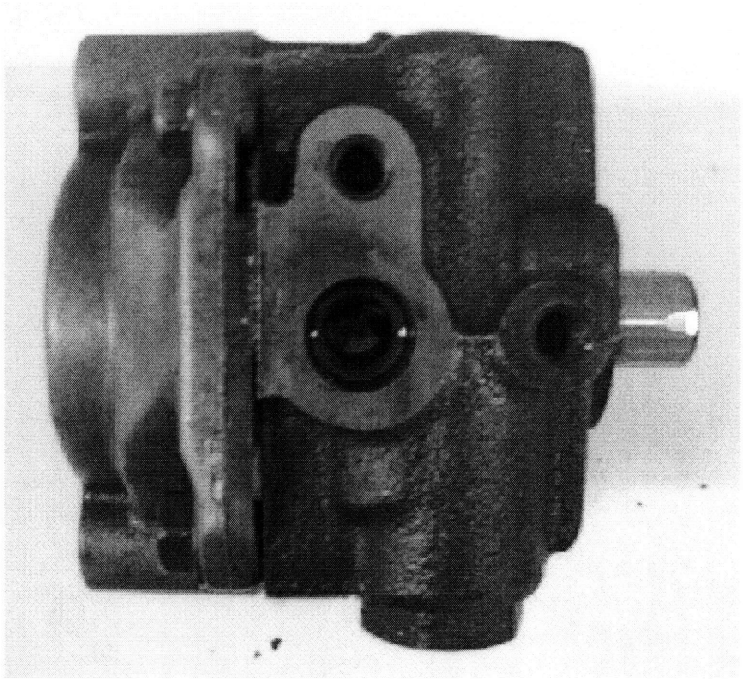

**Figure A. 7: Picture of Pump11**

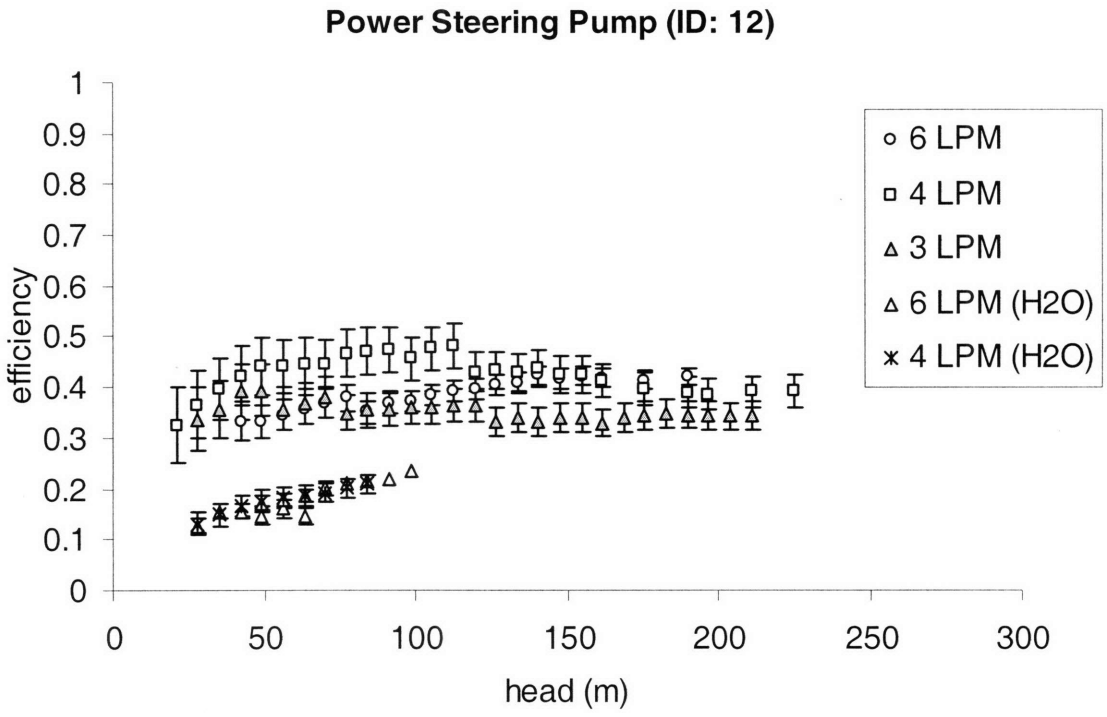


**Figure A. 8: Pump12 pump performance curve**

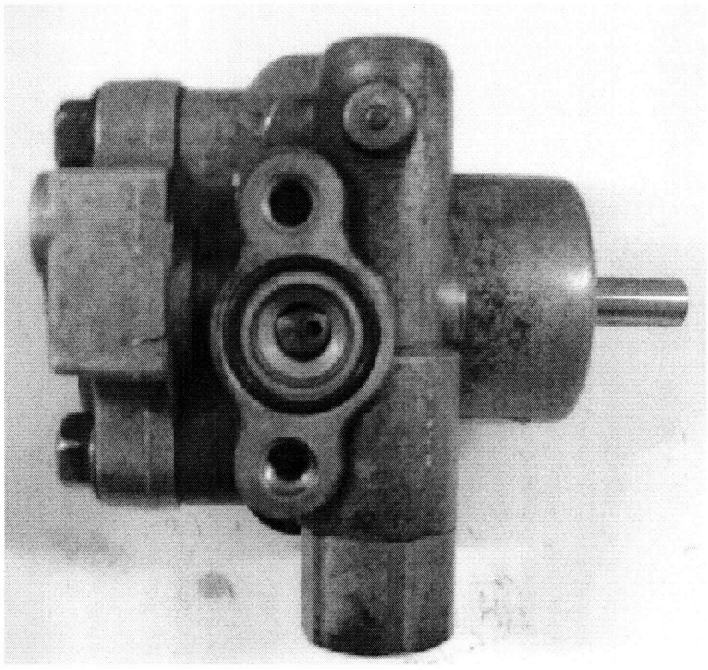

**Figure A. 9: Picture of Pump12**

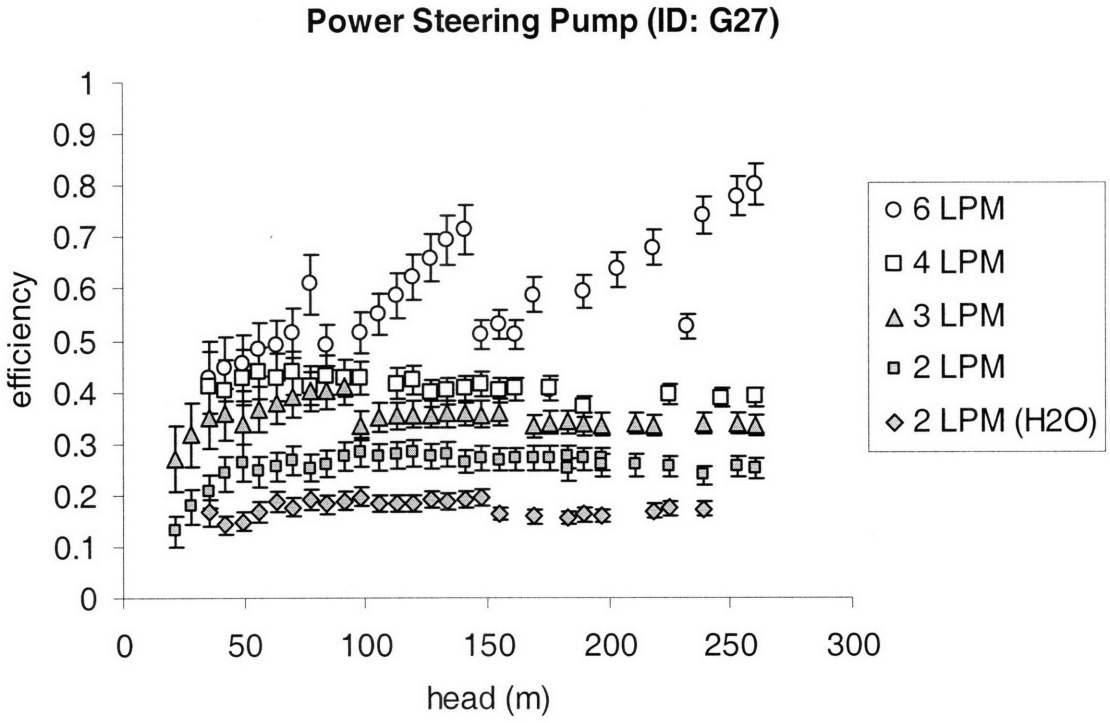


**Figure A. 10: Pump27 pump performance curve**

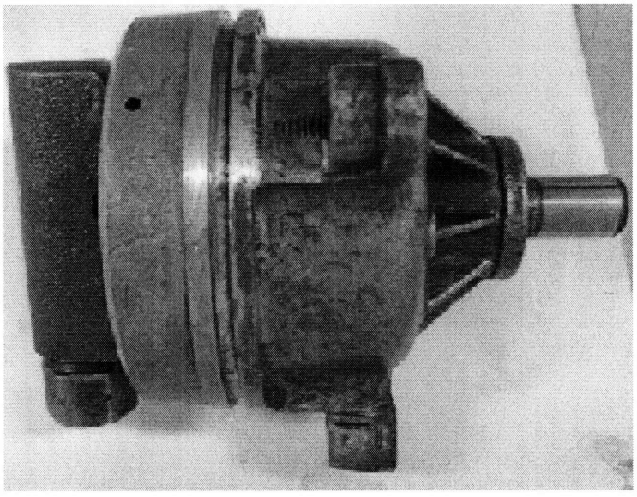

**Figure A. 11: Picture of PumpG27**

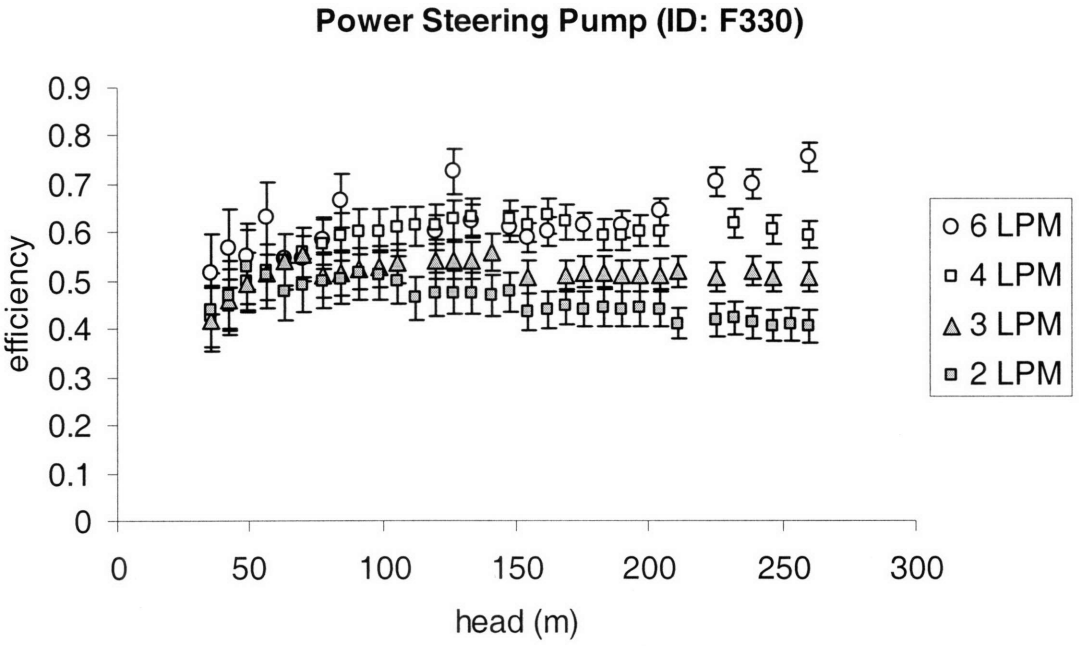


**Figure A. 12: PumpF330 pump performance curve**

**Figure A. 13: Picture of PumpF330**

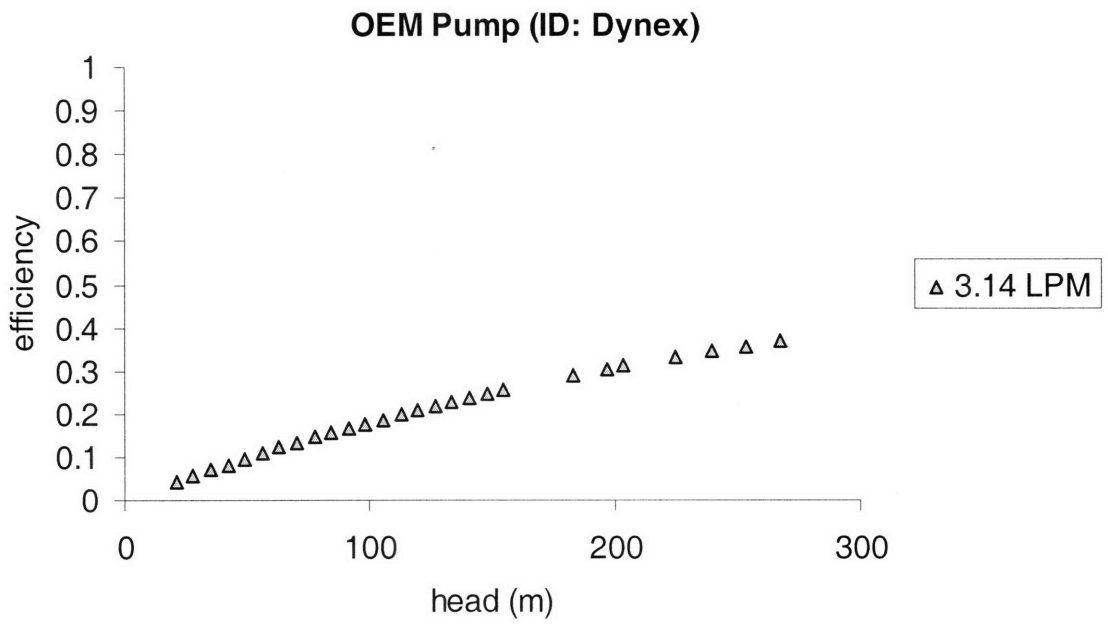


**Figure A. 14: Dynex pump performance curve**

Note: PumpDynex runs at a fixed flow rate of 3.14 LPM because it is attached to a motor with a fixed 1725 rpm

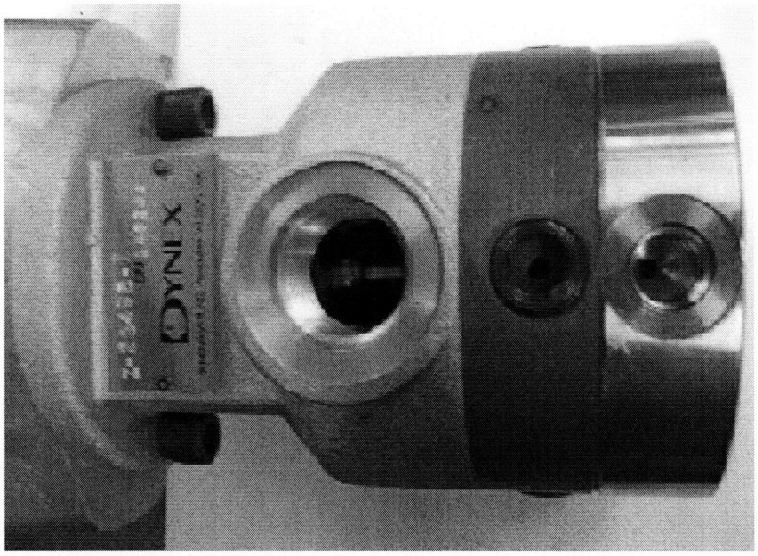


**Figure A. 15: Picture of Dynex pump**

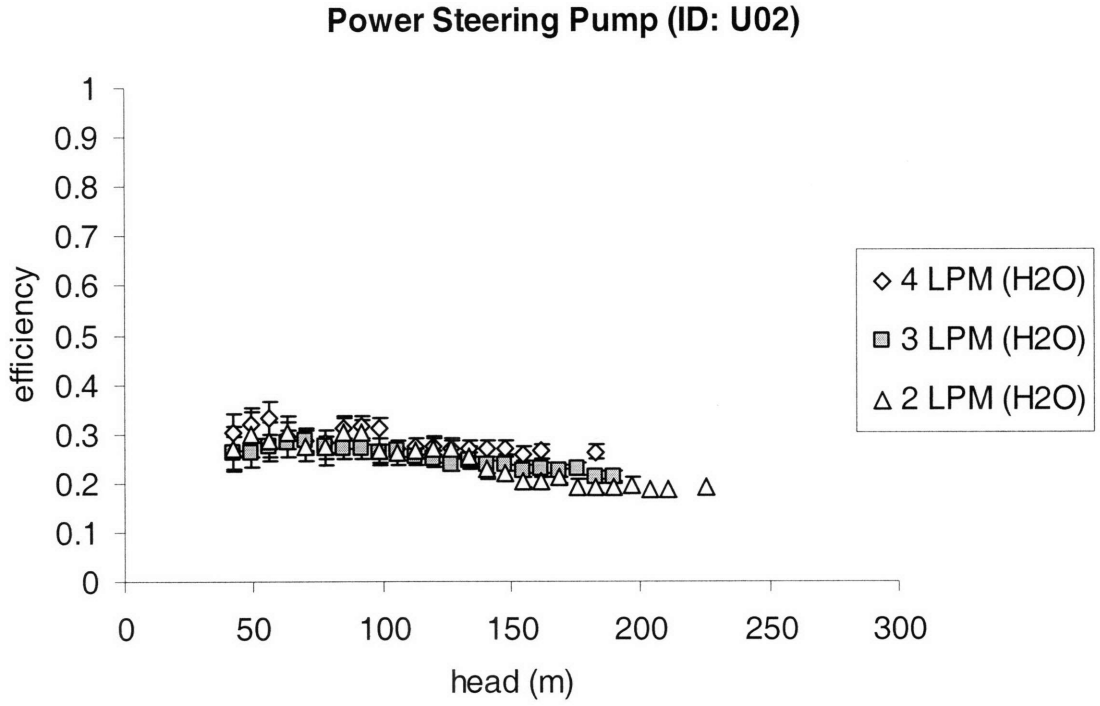


**Figure A. 16: PumpU02 pump performance curve**

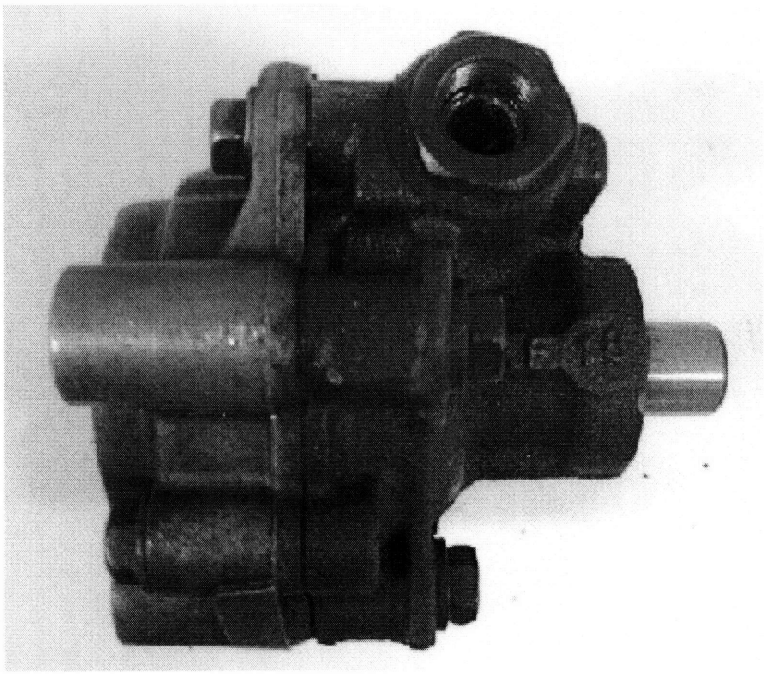

**Figure A. 17: Picture of PumpU02**

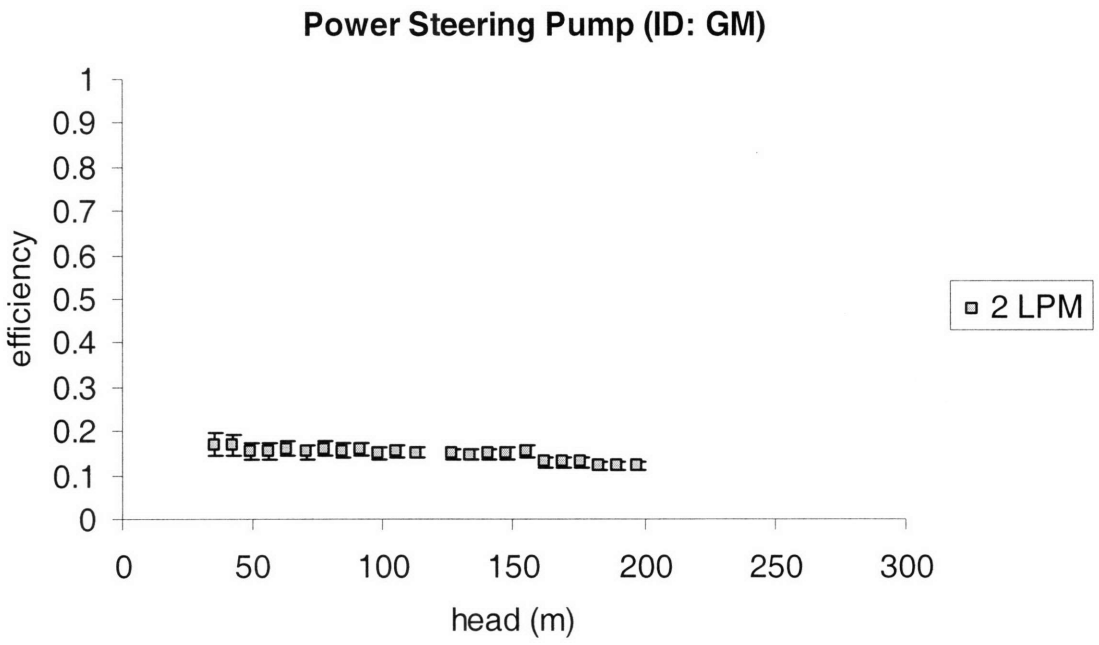


**Figure A. 18: PumpGM pump performance curve**

Note: The shaft seal on PumpGM failed, so the pump was broken after the first trial

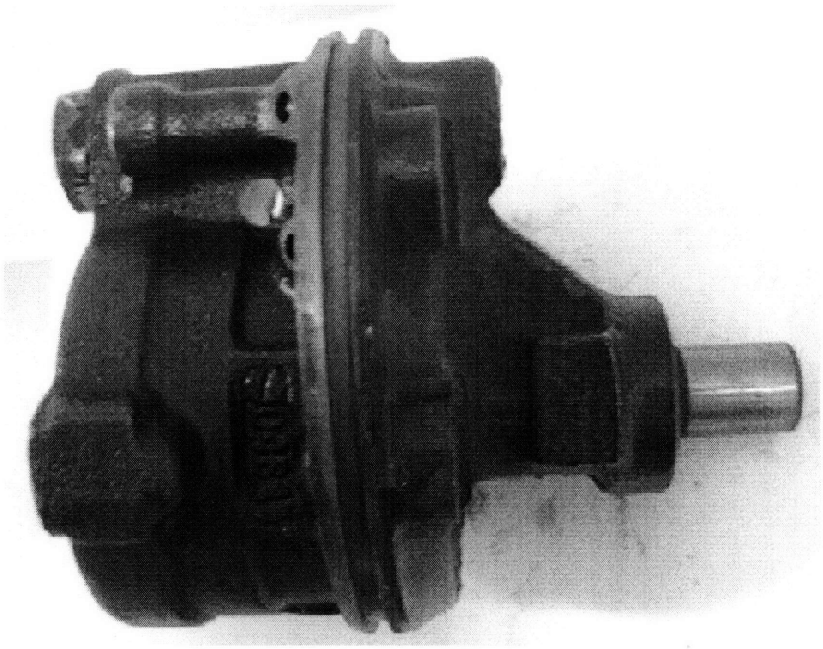

**Figure A. 19: Picture of PumpGM**